Bulletin of Earthquake Engineering (2025) 23:2377–2420
https://doi.org/10.1007/s10518-025-02135-8

ORIGINAL ARTICLE

Unified force-based design approach for the seismic analysis and design of liquid storage tanks

Soumitra Chatterji[1] · **Christoph Butenweg**[2] · **Sven Klinkel**[1]

Received: 7 August 2024 / Accepted: 23 February 2025 / Published online: 10 March 2025

Abstract
Historical observations reveal that Liquid Storage Tanks (LST) have suffered significant earthquake-induced damages. The structural response of LST are sensitive to earthquakes due to dynamic fluid-tank interaction. Since designing with consideration of fluid-tank interaction in the time domain is complex, simplified calculation approaches have been developed to calculate base shear and overturning moments, but not pressure distributions. These approaches distinguish between flexible and rigid tanks, which is difficult to decide prior analysis. This paper presents a unified calculation concept that determines support reactions and pressure distributions independently of the tank's stiffness by applying static equivalent loads. The research focuses on the distinction between rigid and flexible design approaches, review existing codes, their limitations, and challenges associated with relative acceleration response spectra. It scrutinizes varying definitions of impulsive components and superposition principles. A unified force-based design approach is suggested that integrates rigid and flexible design principles into a unified method. The approach uses standardized pressure curves of individual hydrodynamic pressure components, linked with absolute and relative spectral accelerations and appropriate superposition methods. The unified formulation is validated through a previously conducted experimental and numerical research on above-ground steel tank. The validation and application of the unified approach forms the basis for the new generation of Eurocode FprEN 1998-4 (2025), which is demonstrated for different tank geometries. The practical application is demonstrated on a squat and a slender tank using linear finite element model, and the results are compared with various approaches in the international standards and literature.

Keywords Liquid storage tanks · Relative acceleration spectra · Flexibility and rigidity · Unified approach · Eurocode 8

Extended author information available on the last page of the article

1 Introduction

Liquid Storage Tanks (LST) store products like chemicals, fresh and wastewater, petroleum, among others to guarantee uninterrupted supply across processing units in industrial facilities. In past years, there has been a significant rise in the deployment of tanks tailored for cryogenic liquids especially liquid hydrogen (Aziz 2021). LST primarily serve to maintain safety, stability, and serviceability under various loading conditions, including the hydrostatic pressure of stored liquid, earth pressure, temperature variations, wind loads, dead loads, settlements, and earthquakes. Historical observations have indicated that LST have incurred significant damages due to earthquakes (Swan et al. 1985; Yanagisawa et al. 1990; Manos 1991; Erdik 2001; Krausmann and Cruz 2013; González et al. 2013; Brunesi et al. 2015; Yoshida 2018; Erkmen 2024). The predominant outcomes of tank failures are often the leakage of contents (LOC), ignition of fires, detonations, and the emission of toxic gases (Chang and Lin 2006). In certain instances, this phenomenon can lead to technological accidents involving hazardous substances triggering cascading, transboundary, and wide-range impacts (Phan et al. 2020; Paolacci et al. 2024). In general, such interaction between natural hazards and industrial accidents are often referred to as NaTech accidents (Natural Hazards Triggering Technological accidents) (Girgin et al. 2019). The seismic damages of the above-ground steel LST can be diverse and complex (Calvi and Nascimbene 2023). The damage can encompass a spectrum of issues, including failures of tank anchorages, roof and foundation failures, sloshing impacts and spills, shell buckling (elephant's foot, diamond-shaped, local or secondary), uplifting as well as sliding (Natsiavas 1987; Lau and Clough 1989; Rammerstorfer et al. 1990; Schiff 1991).

Under horizontal and vertical seismic excitation, liquid-filled tanks experience hydrodynamic pressures. Calculating these pressures is a complex, iterative, and time-consuming challenge, especially for flexible steel tanks, as it involves the deformation of the tank shell and the interaction between the displaced fluid and the tank wall (Meskouris et al. 2019). A large number of experimental studies focusing on seismic analysis of LST have yielded significant insights (Jacobsen and Ayre 1951; Clough 1977; Clough et al. 1979; Niwa 1978; Manos and Clough 1982; Shih 1981; Shih and Babcock 1987; Park et al. 2016; Caprinozzi et al. 2021). The results of this intensive research have shown that the hydrodynamic effects experienced by flexible tanks during earthquake-induced ground motion can be significantly greater than those experienced by similarly sized rigid tanks due to an additional impulsive flexible pressure. Nevertheless, these studies require a considerable investment of time and resources and have proven to be extravagant. Hence, the necessity for straightforward practical design codes for everyday application became evident as well. Initial investigations into the mathematical depiction of hydrodynamic pressure effects using a rigid tank model by considering impulsive rigid and sloshing pressure components however neglecting the interaction between the tank and the fluid (Jacobsen 1949; Housner 1954, 1963; Epstein 1976; Wozniak and Mitchell 1978). This still remains the basis for seismic analysis in concrete tanks and construction codes such as API650 (2013). The application of the rigid tank design for thin-walled steel tanks frequently resulted in underestimated values for seismic responses. To overcome the limitations many authors (Veletsos 1974; Veletsos and Yang 1977; Veletsos 1984; Veletsos and Tang 1986; Clough 1977; Haroun 1980; Haroun and Housner 1981; Priestley et al. 1986) extended their research to include the flexibility of tank walls in steel tanks which overall increases the induced hydrodynamic pressure due to

inclusion of impulsive flexible components. This also underpins the analytical approach for flexible head-supported cylindrical tanks in nuclear reactors (Yu and Whittaker 2020). Furthermore, Malhotra et al. (2000) and Malhotra (2021) introduced a simplified procedure for the calculation of the base shear and overturning moment using response spectrum method. The aforementioned methods were limited by insufficient data on pressure curves and stress distributions in the tank walls required for stress and stability verification. Fischer, Rammerstorfer and Scharf (1979, 1981, 1982, 1988, 1990a, 1991, 1999, 2004) extended the investigation including the tank wall's flexibility by considering the deformation through an assumed bending shape of the tank wall (Habenberger 2001; Kettler 2004) and thereby modifying the mass or increasing the density in iteration using the added mass model (Holl 1987). However, the derived pressure functions were not directly applicable in practice, as the calculation of the impulsive pressure functions requires the coupling of numerical models with mathematical software packages. Meskouris et al. (2019) developed a finite element application, SALT (Seismic Analysis of Liquid-Filled Tanks), which incorporates the added mass procedure for an effective seismic analysis of tanks. This streamlined the hydrodynamic pressure components for practical application and resulted in the integration of normalized tabulated pressure functions and force coefficients. Furthermore, Holtschoppen and Knoedel (2024) demonstrated that these normalized pressure and force coefficients with certain modifications can also be extended to the design of slender tanks on feet or skirts.

Modern seismic codes, standards, guidelines, and reports for the seismic design of above ground liquid storage steel tanks are numerous with the latest compilation available in Calvi and Nascimbene (2023). However, there exist only two codes (NZSEE 2009 and EN 1998-4 2006) that incorporate flexible tank design by accounting for the impulsive flexible pressure component by considering three pressure components (convective, impulsive rigid and impulsive flexible). However, both codes have limitations. EN 1998-4 (2006) uses a rigorous added-mass method, time history analysis, and complex intricate expressions to calculate impulsive flexible pressure distribution, base shear and overturning moment. Although, the code emphasizes the significance of using relative acceleration for the impulsive flexible component but also acknowledges the lack of a precise method for integrating peak ground acceleration (PGA) with relative acceleration. Scharf (1990a) suggested that absolute and relative response accelerations are similar within the relevant frequency range for tank-fluid dynamics. However, if the distinction between rigid tank and flexible tank is not prior, applying flexible tank design principles to rigid tanks results in an overestimation of stress resultants. Rammerstorfer et al. (1988) proposed various simplified superposition methods for combining the three pressure components, yet the question of which method to adopt remains unresolved. Additionally, constructing and utilizing a relative response spectrum for simplified calculations of impulsive flexible components is a complex task. Conversely, while NZSEE (2009) offers simple formulas and charts for calculating stress resultants but it lacks in evaluating impulsive flexible pressure pressure functions. Additionally, it defines equivalent impulsive masses for rigid and flexible tanks based on a discrete change in the tanks' liquid height to radius ratio H/R based on Veletsos and Yang (1976, 1977, 1984). Although, the authors suggested that for tanks with H/R below 1, a rigid design approach is practical, but the figures and charts were applicable to tanks with a wall thickness to radius ratio s_w/R of 0.001. Therefore, there is a possibility that a squat tank with thinner wall sections may require a flexible design approach. Moreover, Haroun and Housner (1981) proposed that for flexible design, the difference in impulsive masses should be considered

when calculating the rigid impulsive mass to estimate stress resultants. This again presents a significant drawback in maintaining consistency in the definitions and effects of impulsive rigid and flexible components.

The paper seeks to address several critical questions: Firstly, is the distinction between rigid and flexible tanks essential, and if not, how can these categories be effectively integrated for liquid storage steel tanks? Secondly, what are the reasons behind the changing definitions of impulsive components and superposition principles across different tank geometries? Therefore, the research presents a unified force-based design approach for the calculation of seismic support reactions and pressure distributions independently of the tank's stiffness. The main objective is to set forward a consistent definition of the impulsive pressure components in the rigid or flexible design approach. The approach is based on standardized pressure curves of individual hydrodynamic pressure components, linked with corresponding absolute and relative spectral accelerations and superimposed using appropriate superposition methods. The validation and application of the unified approach, which also forms the basis for the new generation FprEN 1998-4 (2025) is demonstrated for different tank geometries. The paper outlines the basics and key terminology in the seismic analysis of LST in Chapter 2, while Chapter 3 presents the seismic response spectra, specifically addressing the aspect of applying relative acceleration response spectra. Chapter 4 discusses the force-based approach for steel tanks and introduces the unified force-based approach followed by a parametric study. The formulation undergoes a two-stage validation in Chapter 5, culminating in a practical application through a quasi-static FEM evaluation in Chapter 6, and is compared with existing approaches for a squat and a slender tank.

2 Seismic analysis of liquid storage tanks

An above-ground, vertical, cylindrical and anchored tank shown in Fig. 1 is the most common case in practice. All hydrodynamic pressure components for tanks can be derived from the streaming potential Φ for fluids under the assumption of a frictionless, irrotational flow and incompressibility of the liquid. This is achieved satisfying three boundary conditions: radial velocity along the tank wall, axial velocity at the tank bottom, and sloshing constraint at the liquid surface with pressure at the free surface (Sigloch 2012).

The following notations and formulae use the following variables:

R inner radius of the tank wall;
H liquid filling height;
L tank length including freeboard;
ξ dimensionless radius, $\xi = r/R$;
ζ dimensionless height, $\zeta = z/H$;
θ circumferential angle;
γ radius to the filling height ratio, $\gamma = H/R$;
ρ_L density of the liquid;
$s_w(\zeta)$ wall thickness;
$f(\zeta)$ fundamental joint natural bending mode shape of tank and liquid;
η radius to wall thickness ratio, $\eta = R/s_w$.

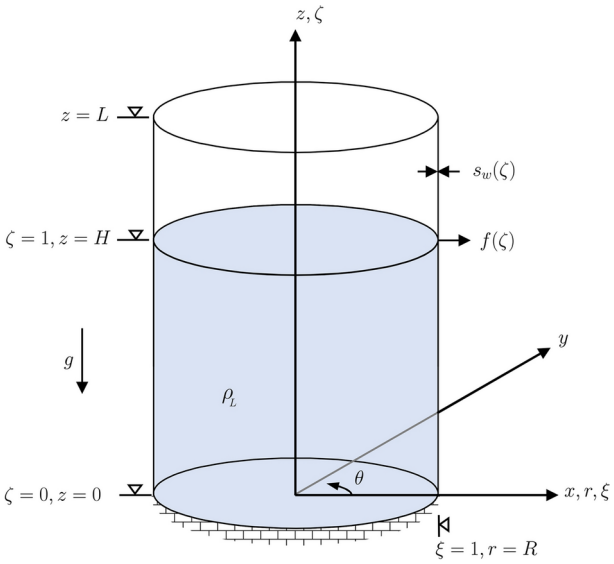

Fig. 1 Geometric model of an above-ground, vertical, cylindrical, anchored tank

The Fourier product of the potential function Φ ensure that each partial function (P, S, Q, F) is dependent on a single variable: radial ξ, axial ζ, circumferential θ, and time t respectively (Hackbusch et al. 2003):

$$\Phi(\xi, \zeta, \theta, t) \;=\; P(\xi)\; S(\zeta)\; Q(\theta)\; F(t) \tag{1}$$

The assumption of a symmetrical velocity potential allows the use of a Fourier series with cosine terms for $Q(\theta)$ in circumferential direction:

$$Q(\theta) \;=\; \sum_{m=0}^{\infty} Q_m cos(m\theta) \tag{2}$$

The time-dependent function $F(t)$ is determined by the corresponding inhomogeneous boundary condition, while the two ordinary decoupled remains in $S(\zeta)$ and $P(\xi)$:

$$\frac{1}{S(\zeta)} \frac{\partial^2 S(\zeta)}{\partial \zeta^2} \;=\; \lambda^2 \tag{3}$$

$$\xi^2 \frac{\partial^2 P(\xi)}{\partial \xi^2} + \xi \frac{\partial P(\xi)}{\partial \xi} + \left(\lambda^2 \xi^2 - m^2\right) P(\xi) = \; 0 \tag{4}$$

Equation 4 describes the radial component is a Bessel differential equation with its derivative roots λ. For solving Eq. 4, the cylindrical Bessel function can be used in numerous mathematical software packages and through the application of boundary conditions of wall and ground deformations, the pressure components acting upon the tank wall and the base of the tank can be calculated.

2.1 One-dimensional horizontal seismic action

Due to horizontal seismic actions, the upper freely moving portion of the liquid content reacts with a sloshing motion, named as convective pressure component (Fig. 2a). Additionally, there are impulsive rigid and flexible modes of vibration that are activated by both horizontal and vertical earthquake excitation. The impulsive rigid vibration component results from the joint rigid body movement of the tank structure with the ground (Fig. 2b). Particularly in the case of flexible steel tanks, the flexural joint vibration causes an interaction between the fluid and the tank wall, resulting in an impulsive flexible vibration (Fig. 2c).

It should be noted that only the first fundamental period is considered in the following calculations of the pressure components. Typically, only relatively slender tanks can have a significant contribution from higher modes. Furthermore, it is assumed that only the first circumferential harmonic of the tank is activated (Fischer 1981; Rammerstorfer et al. 1990; EN 1998-4 2006). This implies that the tank cross-sections remain circular during vibration, and no ovalization effects occur. The assumption describes the tank's behavior as a beam, more specifically as a vertical cantilever beam, where shear deformations are taken into account. Considering only the first circumferential harmonic is sufficiently accurate for slender tanks (Veletsos and Yang 1977). For squat tanks with a value of less than $\gamma = 0.5$, the accuracy of the solutions decreases.

2.1.1 Convective pressure component

A sloshing vibration in the tank is due to a horizontal seismic excitation if the surface of the liquid is allowed to move freely. The coupling between the sloshing and shell vibration modes is usually insignificant, except for weak tanks with large radii. Consequently, the convective dynamic pressure may be calculated according to Eq. 5 by assuming that the tank wall is rigid and that the convective pressure can only be calculated from the fundamental sloshing mode with convective participation factor $\Gamma_c = 1.0$ (Fischer and Rammerstorfer 1999). If the eigenperiod of the oscillating liquid is known, the spatial-temporal variation of the convective pressure distribution can be written as given in Eq. 5:

$$p_c(\xi,\zeta,\theta,t) = R\,\rho_L \left[\frac{2}{\left(\lambda_1{}^2-1\right)}\left\{\frac{J_1(\lambda_1\xi)}{J_1(\lambda_1)}\right\}\left\{\frac{cosh(\lambda_1\gamma\zeta)}{cosh(\lambda_1\gamma)}\right\}\right][cos\theta]\;[\ddot{x}_c(t)] \quad (5)$$

with:

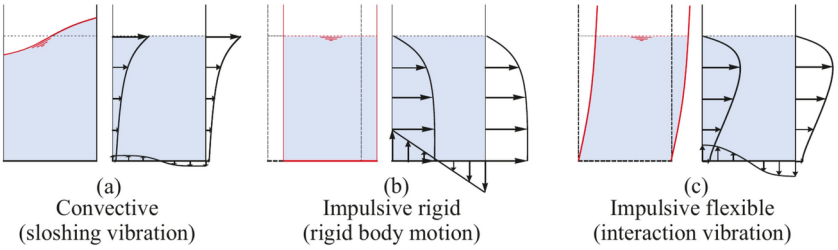

Fig. 2 Qualitative representation of seismically induced hydrodynamic pressure due to horizontal seismic excitation

p_c convective pressure component due to horizontal excitation;
λ_1 first root of the derivative of the Bessel function J_1, $\lambda_1 = 1.841$;
J_1 first order Bessel function (Hackbusch et al. 2003);
$\ddot{x}_c(t)$ horizontal response acceleration time history of the equivalent single-degree-of-freedom (SDOF) oscillator with the time period T_c of the fundamental natural mode. The damping of sloshing fluid ranges between 0 and 0.5%. In case of the response spectrum method $\ddot{x}_c(t)$ is substituted with the elastic spectral acceleration $S_{abs}(T_c)$;
$S_{abs}(T_c)$ absolute spectral acceleration of the elastic response spectrum calculated with damping factor ranging from 0 - 0.5%.

The eigenperiod of the first sloshing mode T_c, can be calculated as given in Eq. 6 according to (Fischer and Rammerstorfer 1982; Stempniewski 1990) with the acceleration due to gravity as g:

$$T_c = \left[\frac{2\ \pi}{\sqrt{\lambda_1 g\ tanh\left(\lambda_1 \gamma\right)}} \right] \sqrt{R}\ or\ C_c \sqrt{R} \tag{6}$$

2.1.2 Impulsive rigid pressure component

The impulsive rigid pressure component is the hydrodynamic pressure caused by the horizontal rigid movement of the tank together with the liquid. The spatial-temporal variation of the impulsive rigid pressure distribution can be written as Eq. 7:

$$p_{ir,h}\left(\xi, \zeta, \theta, t\right) = R\ \rho_L \left[\sum_{n=0}^{\infty} \frac{2\gamma\ (-1)^n}{{\nu_n}^2} \left\{ \frac{I_1\left(\frac{\nu_n}{\gamma}\xi\right)}{I_1'\left(\frac{\nu_n}{\gamma}\right)} \right\} cos\left(\nu_n \zeta\right) \right] \left[cos\theta\right]\ \left[\ddot{x}_{ir,h}\left(t\right)\right] \tag{7}$$

with:
$p_{ir,h}$ impulsive rigid pressure component due to horizontal excitation;
n summation index;
ν_n coefficient: $\nu_n = \frac{2n+1}{2}\pi$;
I_1 modified first order Bessel function; Bessel function with purely imaginary argument (Hackbusch et al. 2003);
I_1' derivative of the first order Bessel function;
$\ddot{x}_{ir,h}(t)$ horizontal acceleration time history for rigid movement (free field or ground acceleration). In case of the response spectrum method $\ddot{x}_{ir,h}(t)$ is substituted with the ordinate of the reduced spectrum in horizontal direction $S_{abs}(T_{ir,h})$ at period $T_{ir,h} = 0$ s. The multiplication with the impulsive rigid participation factor $\Gamma_{ir,h}$ is not applicable as rigid tank moves together with the subsoil i.e. $\Gamma_{ir,h} = 1$.

2.1.3 Impulsive flexible pressure component

The interaction of the liquid content and tank shell results in the impulsive flexible pressure component. The deformation shape of the tank wall is related to the tank geometry, liquid

filling height and its characteristics. The initial deformation function is usually unknown. Therefore, to determine the fundamental time period and the associated mode shape of the tank-liquid system, it is required to solve the eigenvalue problem (Meskouris et al. 2011). The calculation can be carried out using added mass model (Rammerstorfer et al. 1988; Fischer et al. 1991; EN 1998-4 2006). The deformation profile of the "dry" shell with added density is then calculated (Meskouris et al. 2011). With knowledge of the deformation shapes of the tank shell $f(\zeta)$, the impulsively flexible pressure component due to horizontal earthquake excitation can be calculated as given in Eq. 8:

$$p_{if,h}\left(\xi,\zeta,\theta,t\right)=R\ \rho_L\ \left[\sum_{n=0}^{\infty}\frac{2}{\frac{\nu_n}{\gamma}}\ \left\{\frac{I_1\left(\frac{\nu_n}{\gamma}\xi\right)}{I'_1\left(\frac{\nu_n}{\gamma}\right)}\right\}\ cos\left(\nu_n\zeta\right)\int_0^1 f\left(\zeta\right)\ cos\left(\nu_n\zeta\right)\right]\cdot \tag{8}$$
$$[cos\theta]\ \ [\ddot{x}_{if,h}\left(t\right)]$$

with:

$p_{if,h}$ impulsive flexible pressure component due to horizontal excitation;
$f\left(\zeta\right)$ fundamental joint natural bending mode shape of tank and liquid;
$\ddot{x}_{if,h}$ relative horizontal acceleration time history of the equivalent SDOF oscillator of the joint bending vibration of tank and liquid. In case of the response spectrum method $\ddot{x}_{if,h}(t)$ is substituted by the difference in spectral acceleration in horizontal direction $\left[S_{abs}\left(T_{if,h}\right)-S_{abs}\left(T_{ir,h}\right)\right]\cdot\Gamma_{if,h}$;
$\Gamma_{if,h}$ participation factor corresponding to the fundamental flexible horizontal natural mode.

The impulsive flexible pressure $p_{if,h}$ (Eq. 8) demands the choice of bending shape function $f\left(\zeta\right)$. EN1998-4 (2006) did not explicitly provide a shape function, except stating a single comment that the bending shape proportional to ζ is a good approximation for slender tanks. Habenberger (2001) and Kettler (2004) set forth the possible approximation for the bending shape $f(\zeta)$, by means of sine-shaped function $f\left(\zeta\right)\ =\ sin\left(\pi/2\cdot\zeta\right)$ for squat tanks ($\gamma<3$), a linear shaped function $f\left(\zeta\right)\ =\ \zeta$ for slender tanks ($3\le\gamma\le8$) and cosine shaped function $f\left(\zeta\right)\ =1-cos\left(\pi/2\cdot\zeta\right)$ for very slender tanks ($\gamma>8$). However, the hydrodynamic pressure curves, equivalent impulsive masses and heights exhibits a lack of smooth transition in between the changing shape functions. Therefore, the joint bending vibration of the tank and the liquid is approximated using a single sine function with four free parameters a, b, c, d (Cornelissen 2010; Meskouris et al. 2011). These parameters are derived with a Poisson's ratio of ν = 0.3 (steel) and for a constant wall thickness without considering the mass of the tank shell. With these parameters, the function can be scaled and adjusted in both coordinate directions for ratios γ = 1.0 to 10.0. The proposed parametrized sine function depending on the ratio γ is given in Eq. 9:

$$f\left(\zeta\right)\ =a\cdot sin\left(\frac{\pi}{2}\cdot\left(\zeta-b\right)\cdot c\right)+d \tag{9}$$

For ratios lower than $\gamma=1.0$ the approximation based on a sine-shaped function $f\left(\zeta\right)=sin\left(\pi/2\cdot\zeta\right)$ is used. With the proposed shape functions, a good conformity with numerical calculations can be achieved. The proposed functions can serve as known bending mode shapes, eliminating the need for time-consuming iterations. The impulsive flexible

period $T_{if,h}$ can be calculated with FE models. Alternatively, the first eigenperiod $T_{if,h}$ can be calculated according to Rammerstorfer et al. (1988) given in Eq. 10:

$$T_{if,h} = 2RF_h(\gamma)\sqrt{\frac{\rho_L H}{E s_w\left(\zeta = \frac{1}{3}\right)}} \tag{10}$$

with:

$F_h(\gamma)$ correction factor: $F_h(\gamma) = 0.157\,\gamma^2 + \gamma + 1.49$;

E Young's modulus of the tank shell;

$s_w\,(\zeta = 1/3)$ thickness of the tank shell at $\frac{1}{3}^{rd}$ of the filling height.

2.2 One-dimensional vertical seismic action

The mathematical derivations for the vertical hydrodynamic pressure components can be found in Luft (1984), Fischer and Seeber (1988) and Tang (1986). Figure 3 shows the tanks vertical movement and the associated impulsive pressure distributions that are rotational symmetrical in circumferential direction.

2.2.1 Impulsive rigid pressure component

Figure 3a shows the vertical tank movement and the rotational symmetrical pressure distribution on the tank wall. According to Fischer et al. (1991) the impulsive rigid pressure component can be calculated as given in Eq. 11.

$$p_{ir,v}(\zeta, t) = R\,\rho_L\,[(1-\zeta)\,\gamma]\,[\ddot{x}_{ir,v}(t)] \tag{11}$$

with:

$\ddot{x}_{gv}(t)$ vertical acceleration time history for rigid movement. In case of the response spectrum method $\ddot{x}_{ir,v}(t)$ is substituted by the vertical spectral acceleration $S_{abs}(T_{ir,v}) \cdot \Gamma_{ir,h}$ at period $T_{ir,v} = 0$ s;

$\Gamma_{ir,v}$ Participation factor of the impulsive rigid pressure component, $\Gamma_{ir,v} = 1$ as the entire tank moves in unison with the vertical ground movement.

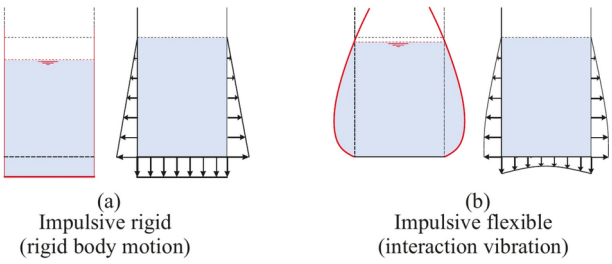

Fig. 3 Qualitative representation of seismically induced hydrodynamic pressure due to vertical seismic excitation

2.2.2 Impulsive flexible pressure component

Tang (1986) and Habenberger (2001) showed that the rotationally symmetric impulsive flexible pressure component is due to the elasticity of a flexible tank wall. Figure 3b shows the bending vibration mode with the corresponding qualitative pressure distribution on the tank wall. According to Scharf (1990b) and Habenberger (2001), the impulsive flexible pressure component due to vertical excitation is given by Eq. 12.

$$p_{if,v}\left(\xi,\zeta,t\right)=R\ \rho_L\left[\gamma\frac{2}{\pi}\left\{\frac{I_0\left(\frac{\pi}{2\gamma}\xi\right)}{I_1\left(\frac{\pi}{2\gamma}\right)}\right\}\beta\left(\gamma\right)cos\left(\frac{\pi}{2}\zeta\right)\right]\ \left[\ddot{x}_{if,v}\left(t\right)\right] \tag{12}$$

with:

I_0, I_1 modified Bessel functions of zero and first order;

$\beta(\gamma)$ correction factor taking account of the clamping effect as: $\beta(\gamma) = 1.0$ for $\gamma \leq 0.8$; $\beta(\gamma) = 1.078 + 0.274\ ln\ (\gamma)$ for $0.8 < \gamma \leq 4$;

$\ddot{x}_{if,v}\left(t\right)$ vertical acceleration time history of the joint vibration of the tank and the liquid. In case of the response spectrum method $\ddot{x}_{if,v}(t)$ is substituted with the difference in spectral acceleration in vertical direction $\left[S_{abs}\left(T_{if,v}\right)-S_{abs}\left(T_{ir,v}\right)\right]\cdot\Gamma_{if,v}$;

$\Gamma_{if,v}$ participation factor of the impulsive flexible pressure component due to vertical excitation; $\Gamma_{if,v}=\frac{4}{\pi}\left\{I_1\left(\frac{\pi}{2\gamma}\right)/I_0\left(\frac{\pi}{2\gamma}\right)\right\}$.

The fundamental natural period $T_{if,v}$ can be calculated according to Rammerstorfer and Fischer (2004) as given in Eq. 13:

$$T_{if,v}\ =2R\ F_v\left(\gamma\right)\sqrt{\frac{\rho_L H\left(1-\nu^2\right)}{Es_w\left(\zeta=\frac{1}{3}\right)}} \tag{13}$$

with:

ν Poisson's ratio of the tank shell;

$F_v(\gamma)$ correction factor: $F_v\ =\sqrt{2\pi\left\{I_0\left(\frac{\pi}{2\gamma}\right)/I_1\left(\frac{\pi}{2\gamma}\right)\right\}}$.

2.3 Simplification of the pressure components

The pressure functions defined in Sect. 2.1 and Sect. 2.2 are naturally not easy to apply in everyday practice as the static equivalent loads of the pressure components are based on the integration of Bessel functions. Furthermore, the calculation of the impulsive flexible pressure necessitates a iterative eigenvalue analysis of the tank to approximate the bending mode. A simplification of the application can be achieved with dimensionless pressure functions at the tank wall and bottom. This is calculated by considering the first vibration mode and by normalizing the pressure functions derived in Sects. 2.1 and 2.2 in horizontal direction with $R\ \rho_L\ cos\theta\ S_{ah}(T_j)\ \Gamma_j$ and in vertical direction with $R\ \rho_L\ S_{av}\left(T_k\right)\Gamma_k$ (see

Eqs. 14, 15). Therefore, a simplification of the five pressure components (Eqs. 5, 7, 8, 11, 12) is attained by integrating and compiling the Bessel series expansions i.e. the expression inside the closing bracket [ ] to 100 terms in the form of coefficients $C_j(\gamma,\zeta)$ and $C_k(\gamma,\zeta)$ for estimating wall pressures and $C_{b,j}(\gamma,\xi)$ and $C_{b,k}(\gamma,\xi)$ use for estimating base pressures. The three horizontal pressure components (convective, impulsive rigid, impulsive flexible) shown in Sect. 2.1 and two vertical pressure components (impulsive rigid, impulsive flexible) shown in Sect. 2.2 can be simplified with the coefficients for horizontal and vertical seismic excitation as given in Eqs. 14 and 15 respectively. It should be emphasized that the wall coefficients and base coefficients are mutually exclusive and cannot be applied simultaneously.

$$p_j(\xi,\zeta,\theta) = R \cdot \rho_L \cdot \left[\underbrace{C_j(\gamma,\zeta)}_{\text{for wall pressure}} \quad or \quad \underbrace{C_{b,j}(\gamma,\xi)}_{\text{for base pressure}} \right] \cdot cos\theta \cdot S_{ah}(T_j) \cdot \Gamma_j(\gamma) \tag{14}$$

$$p_k(\xi,\zeta) = R \cdot \rho_L \cdot \left[\underbrace{C_k(\gamma,\zeta)}_{\text{for wall pressure}} \quad or \quad \underbrace{C_{b,k}(\gamma,\xi)}_{\text{for base pressure}} \right] \cdot S_{av}(T_k) \cdot \Gamma_k(\gamma) \tag{15}$$

with:

p_j	pressure component due to horizontal excitation $j = \{c;\ ir,h;\ if,h\}$;
p_k	pressure component due to vertical excitation $k = \{ir,v;\ if,v\}$;
C_j, C_k	tabulated coefficients of pressure component p_j and p_k respectively;
S_{ah}, S_{av}	horizontal and vertical spectral acceleration of the pressure component p_j and p_k respectively;
T_j, T_k	fundamental natural period of the equivalent SDOF oscillator of the pressure component p_j and p_k respectively;
Γ_j, Γ_k	participation factor of the pressure component p_j and p_k respectively.

Fig. 4 shows an overview of all the wall and base pressure coefficients for different γ due to horizontal seismic excitation. The convective wall pressure coefficient C_c shown in Fig. 4a peaks at 0.8371 at the liquid surface's apex and decreases towards the tank base. The impulsive rigid wall pressures coefficient $C_{ir,h}$ (Fig. 4b) peaks at the tank base. In squat tanks (low γ), impulsive flexible wall pressure coefficient $C_{if,h}$ are uniformly distributed (Fig. 4c), but in tanks with high γ, these coefficients primarily impact the upper half of the wall. The base pressure coefficients decreases for convective and increases for impulsive rigid pressures as γ rises up to 5.0 (Fig. 4 d_1 to e_2). Beyond $\gamma = 5.0$, convective base pressures drop to zero, while impulsive rigid pressures peak at 1 at the tank's diameter end. The impulsive flexible base pressure coefficient $C_{b,if,h}$ increase up to $\gamma = 1.0$ (Fig. 4f_1) and then decrease (Fig. 4f_2). This pattern is attributable to the impulsive flexible pressure inducing greater bending in the upper half of the tank wall and lesser concentration towards the lower half, as depicted in Fig. 4c. Notably, wall and base coefficients converge at the base of the tank wall i.e. $C_j(\gamma,\zeta=0) = C_{b,j}(\gamma,\xi=1)$. Figure 5 shows an overview of all the wall and base pressure coefficients for different γ due to vertical seismic excitation. For the impulsive rigid component, the wall coefficient $C_{ir,v}$ varies linearly with γ, while the base coefficient $C_{b,ir,v}$ remains constant (Fig. 5 a_1 to a_2). The impulsive flexible component

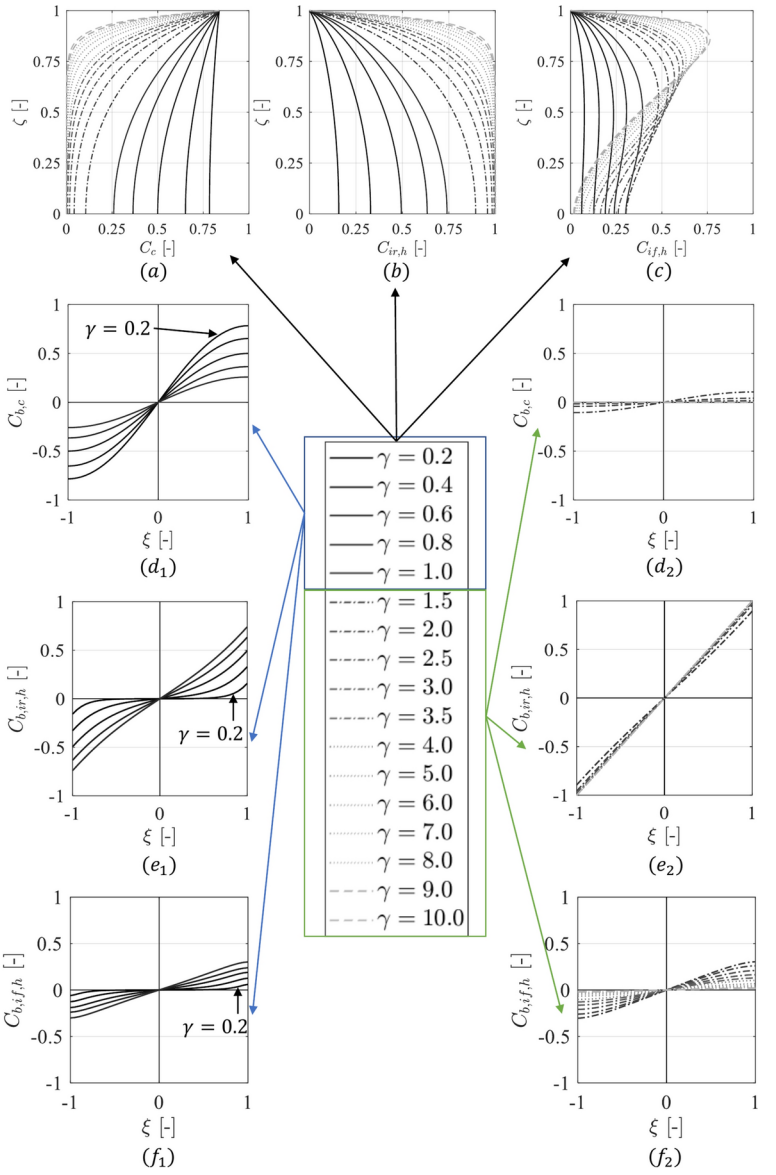

Fig. 4 Convective, impulsive rigid and impulsive flexible coefficients for different γ use for calculating (**a**–**c**) wall pressures and (**d**–**f**) base pressures due to horizontal seismic excitation

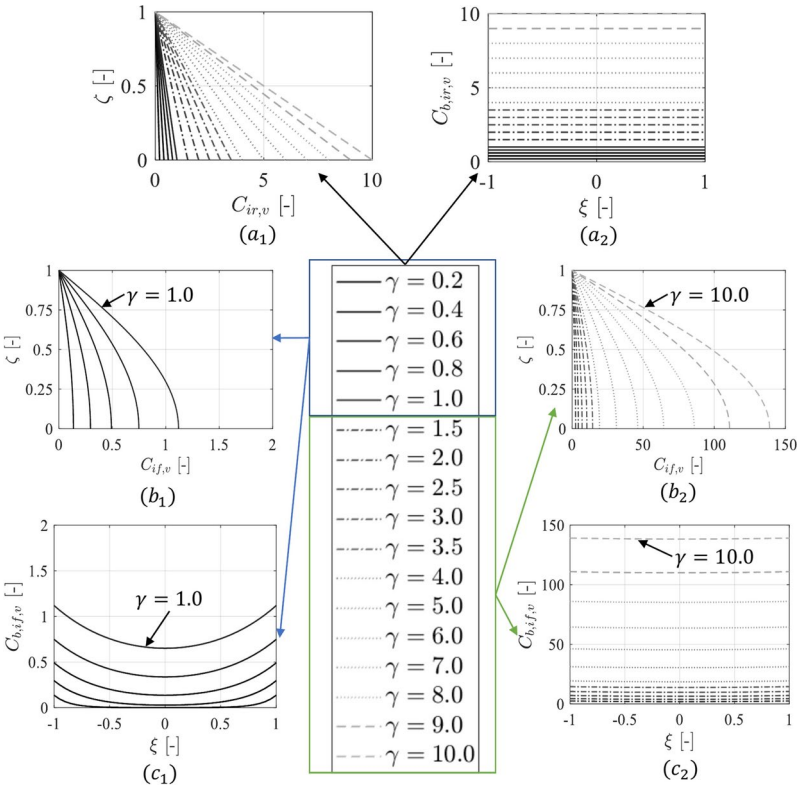

Fig. 5 Impulsive flexible pressure coefficients for different γ use for calculating (**a**) impulsive rigid wall and base pressures and (**b**, **c**) impulsive flexible wall and base pressures due to vertical excitation

shows wall coefficients $C_{if,v}$ following the tank's radial breathing mode (Fig. 5 b_1 to b_2) whereas the base coefficients $C_{b,if,v}$ vary non-uniformly, being minimal at the center and maximal at the edges (Figs. 5 c_1 and c_2). Here also the wall and base coefficients converge at the base of the tank wall i.e. $C_k\,(\gamma, \zeta = 0) = C_{b,k}\,(\gamma, \xi = 1)$. These wall and base pressure coefficients for horizontal and vertical seismic actions are now formally tabulated in the new FprEN 1998-4 (2025) code.

2.4 Base shear and overturning moment

The calculation of base shear and overturning moment resulting from earthquake loads is needed for the tank foundation design. It is crucial to identify each hydrodynamic component mass and height such that total earthquake forces acting on the tank can be calculated along with the inertia forces. The spring mass model and notations according to FprEN 1998-4 (2025) for above-ground tanks under horizontal seismic actions are shown in Fig. 6 with the following variables:

where

RL rigid link;

m_L is the total liquid mass;

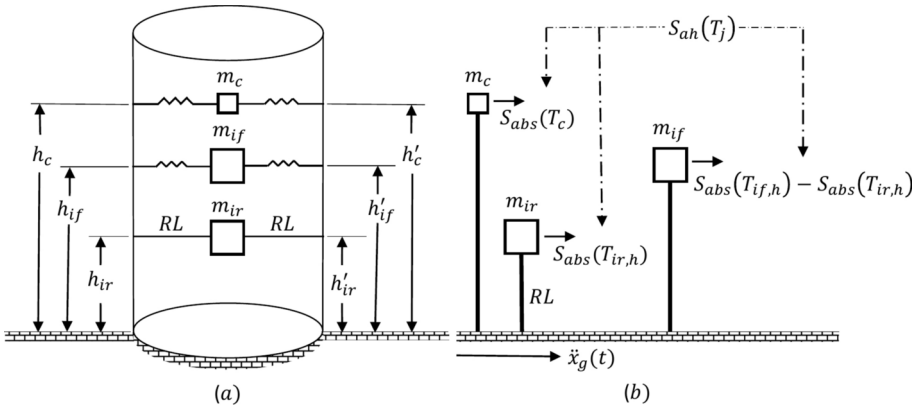

Fig. 6 **a** Spring mass model and notations for tanks under horizontal seismic actions and **b** corresponding spectral accelerations exhibited by each equivalent mass

m_c, m_{ir}, m_{if} are the equivalent convective, impulsive rigid, and impulsive flexible masses;

h_c, h_{ir}, h_{if} are the equivalent lever arms without consideration of the bottom pressure;

h'_c, h'_{ir}, h'_{if} are the equivalent lever arms with consideration of the bottom pressure;

The horizontal and vertical seismic support reactions can also be expressed as derived coefficients. For horizontal seismic action, integrating Eq. 14 along the wall and in circumferential direction leads to the horizontal support reactions (base shear and overturning moments) in the direction of the earthquake. The base shear of the three horizontal pressure components can be calculated as given in Eq. 16:

$$F_{b,j} = \int_{\zeta=0}^{\zeta=1} 2 \int_{\theta=\frac{-\pi}{2}}^{\theta=\frac{\pi}{2}} \left[p_j\left(\xi = 1, \zeta, \theta\right)\right] \; cos\left(\theta\right) \; Rd\theta \; Hd\zeta \tag{16}$$

The overturning moment resulting from the horizontal pressures components acting on the tank wall $p_j\left(\xi = 1\right)$ is given as Eq. 17:

$$M_{w,j} = \int_{\zeta=0}^{\zeta=1} 2 \int_{\theta=\frac{-\pi}{2}}^{\theta=\frac{\pi}{2}} H \; \zeta \; \left[p_j(\xi = 1, \zeta, \theta)\right] \; cos\left(\theta\right) \; Rd\theta \; Hd\zeta \tag{17}$$

The integral expression for the overturning moment resulting from horizontal pressures components on wall $p_j\left(\xi = 1\right)$ and tank bottom $p_j\left(\zeta = 0\right)$ is given as Eq. 18:

$$M_{g,j} = M_{w,j} + \int_{\xi=0}^{\xi=1} 2 \int_{\theta=\frac{-\pi}{2}}^{\theta=\frac{\pi}{2}} \left(R\,\xi\right)^2 \; \left[p_j(\xi, \zeta = 0, \theta)\right] \; cos\left(\theta\right) \; Rd\theta \; d\xi \tag{18}$$

For vertical seismic action, integrating Eq. 15 along the base and in circumferential direction leads to the vertical support reactions. The vertical support reaction of the two vertical pressure components can be calculated as given in Eq. 19:

$$F_k = \int_{\xi=-1}^{\xi=1} \int_{\theta=\frac{-\pi}{2}}^{\theta=\frac{\pi}{2}} \left[p_k\left(\xi, \zeta = 0\right)\right] \; Rd\theta \; Rd\xi \tag{19}$$

After performing the integration, the constant value in the expression are tabulated. The tabulated force and moment coefficients along with the participation factors for each pressure components is introduced for different γ to calculate support reactions. The horizontal support reactions for three pressure components are given in Eq. 20 and the vertical support reaction for two pressure components are given in Eq. 21.

$$\begin{cases} F_{b,j} = C_{F,j} \cdot \Gamma_j \cdot m_L \cdot S_{ah}\left(T_j\right) \\ M_{w,j} = C_{MW,j} \cdot \Gamma_j \cdot m_L \cdot S_{ah}\left(T_j\right) \\ M_{g,j} = C_{M,j} \cdot \Gamma_j \cdot m_L \cdot S_{ah}\left(T_j\right) \cdot (R/\gamma) \end{cases} \tag{20}$$

$$F_k = C_{F,k} \cdot \Gamma_k \cdot m_L \cdot S_{av}\left(T_k\right) \tag{21}$$

with

$C_{F,j}$ base shear coefficient corresponding to the horizontal pressure component p_j with $j = \{c;\ ir,h;\ if,h\}$;

$C_{MW,j}$ overturning moment (wall) coefficient just above the baseplate for the horizontal pressure component p_j

$C_{M,j}$ Overturning moment (wall+base) coefficient just below the baseplate for the horizontal pressure component p_j

$C_{F,k}$ vertical force coefficient corresponding to the vertical pressure component p_k with $k = \{ir,v;\ if,v\}$;

The use of horizontal spectral acceleration for impulsive flexible pressure component as $S_{ah}(T_{if,h}) = S_{abs}(T_{if,h}) - S_{abs}(T_{ir,h})$ is discussed in Chapter 3 and 4 along with the proposed unified force-based design approach.

3 Absolute and relative response spectrum

The absolute acceleration response spectrum $S_{abs}(T, \xi_D)$ is the plot of the peak acceleration response of a spring-dashpot oscillator as function of natural time period T and damping of the system ξ_D for an arbitrary seismic signal as mathematically given in Eq. 22.

$$S_{abs}(T, \xi_D) = |\ddot{x}_{abs}(t)|_{max} = |\ddot{x}_g(t) + \ddot{x}(t)|_{max} \tag{22}$$

The components of absolute time history response acceleration are the ground $\ddot{x}_g(t)$ and relative $\ddot{x}(t)$ acceleration. In view of the flexible design concept for LST, the relative acceleration is an important parameter because of the impulsive flexible pressure component, since the ground acceleration is already accounted in the impulsive rigid pressure component. In order to estimate the seismic demands using force-based approach, the maxima of relative acceleration at any estimated time period is as important as the maxima of ground acceleration. It is critical to note that the maxima of both the components does not signify the maxima of absolute acceleration. In recent country-specific design codes, maximum spectral acceleration $S_{ap,R}$ is used, as in the Euro-Mediterranean Seismic Hazard Model

(Danciu et al. 2021). However, design codes can typically prescribe their own mandatory seismic hazard values in terms of $S_{ap,R}$. PGA is then calculated as $S_{ap,R}/2.5$. The simplified formulation (in spectral form) plugs PGA directly into equations to calculate seismic demands.

The challenge in the flexible design of liquid storage tanks is to use the spectral ground and relative accelerations simultaneously and not change the impulsive components definition. The use of relative acceleration response spectra in seismic analysis of LST is difficult because it may not provide an accurate representation of the actual response of the tank at higher time periods. The use of relative acceleration response spectra may lead to under, equal or overestimates of the true responses of the tank. This is shown in the following study. For investigation, sixty ground motions were selected from PEER ground motion database (Ancheta et al. 2013). Utilizing Newmark's average acceleration method, the absolute and relative acceleration time histories were generated for various time periods of the SDOF system using the open source MATLAB script (Vamvatsikos and Cornell 2004; Vamvatsikos 2011). Figure 7 shows an example plot for the Loma Prieta earthquake (California - October 18, 1989) with a PGA of 0.172g as one of the sixty selected strong ground motions.

For a rigid tank ($T_{if,h} \approx 0\ s$), there are no appreciable $\ddot{x}(t)$ in the system as shown in Fig. 8a and $\ddot{x}_{abs}(t) \approx \ddot{x}_g(t)$. As the flexibility and natural time period of the tank increases, $\ddot{x}(t)$ also increases and later start synchronizing with $\ddot{x}_{abs}(t)$. This overall increase of the tank response is corresponding to dominant increase in relative acceleration of a SDOF system (see Fig. 7b and c). The usage of the word "dominant" is on purpose because the ground acceleration corresponding to max structural response starts decelerating. Further increase in $T_{if,h}$ leads to overall decrease in the amplitude of $\ddot{x}_{abs}(t)$ (see Fig. 7 d and e). This occurs because the relative acceleration $\ddot{x}(t)$ begins to enter a phase reversal in comparison to the ground acceleration $\ddot{x}_g(t)$ (see Fig. 8 d and e). Lastly, $\ddot{x}(t)$ mirrors into $\ddot{x_g}(t)$ in the reverse phase. This observation can be approximately made by comparing the $\ddot{x}_{abs}(t)$ at $T_{if,h} = 0.01\ s$ with the $\ddot{x}(t)$ at $T_{if,h} = 4\ s$ in Fig. 7. Mathematically, this can be expressed $\ddot{x}(t) \approx -\ddot{x}_g(t)$ indicating that the absolute response virtually vanishes due to the phase opposition between the tank's relative acceleration and the ground acceleration as shown in Fig. 8f.

$$S_{rel}(T) = |\ddot{x}(t)|_{max} \tag{23}$$

The absolute $S_{abs}(T)$ and relative $S_{rel}(T)$ spectral accelerations can be calculated using Eqs. 22 and 23 respectively. The peaks in Fig. 7 are selected for different time period to construct the absolute and relative response spectra. Figure 9 shows absolute and relative spectra of SDOF systems for 60 PEER strong ground motion along with mean values. The relative acceleration response spectra $S_{rel}(T)$ start to converge to PGA with increasing time period.

The deception in using the relative response acceleration spectra for flexible tanks can be seen in Fig. 10. For better comprehension, the actual corresponding components of $S_{abs}(T)$ i.e. $\ddot{x}_g(t)$ and $\ddot{x}(t)$ are also shown. It is very clear that the actual relative acceleration $\ddot{x}(t,T)$ that corresponds to $S_{abs}(T)$ is not equal as $S_{rel}(T)$. This is due to the fact that the maxima of two sets ($\ddot{x}_g(t)$ and $\ddot{x}(t)$) of real numbers need not necessary corresponds to the maxima of both sets. Furthemore, at increased time periods, an alteration in the phase of the relative acceleration $\ddot{x}(t,T)$ occurs as also depicted in Fig. 8. Consequently, the absolute maxima

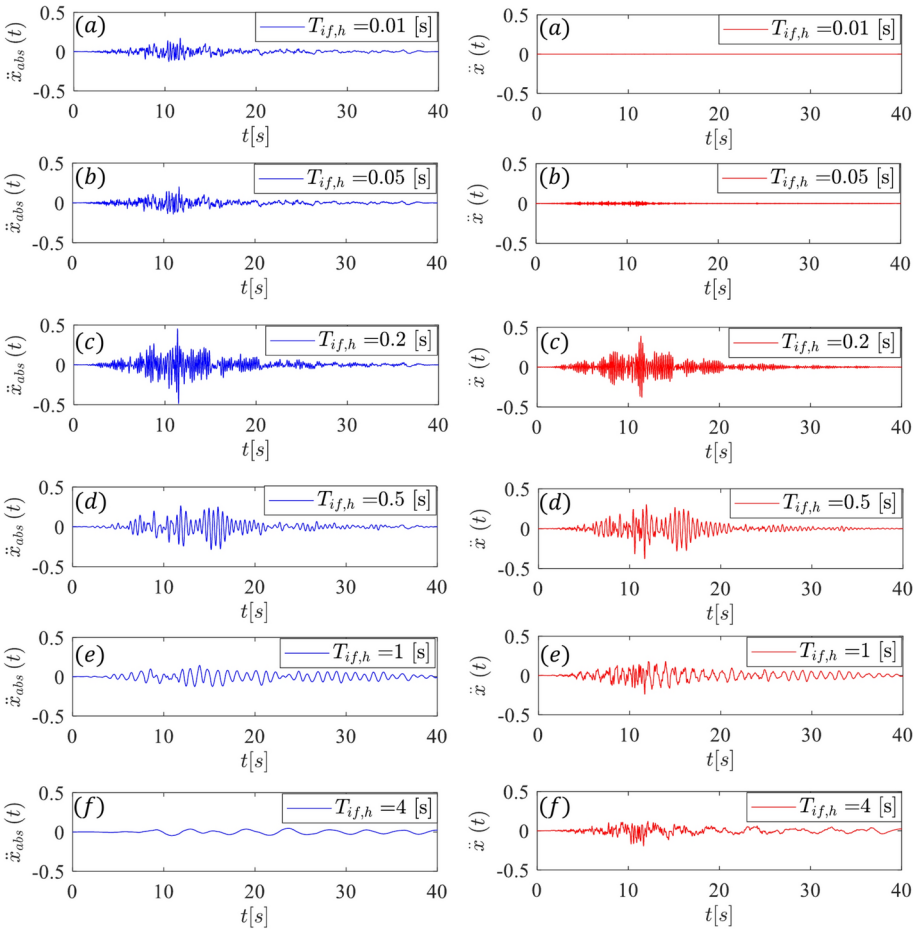

Fig. 7 Absolute (left) and relative (right) acceleration time histories in [g] units with a PGA of 0.172g for different impulsive flexible time periods for the Loma Prieta Earthquake (PEER NGA-West2 Database 2013)

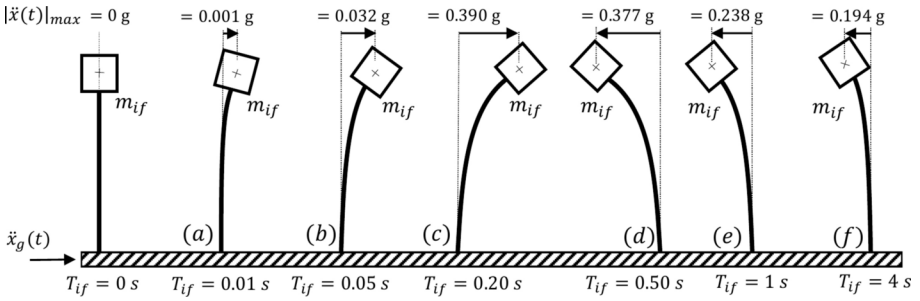

Fig. 8 Maximum relative accelerations of different impulsive flexible time periods for the Loma Prieta Earthquake (PEER NGA-West2 Database 2013) acting at the equivalent impulsive flexible mass

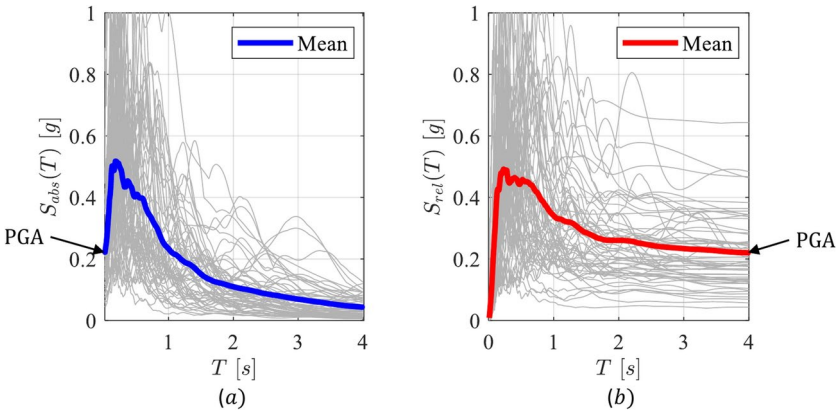

Fig. 9 **a** Mean absolute acceleration response spectra and **b** mean relative acceleration response spectra for different time periods of SDOF system for 60 PEER ground motion from NGA-West2 2013)

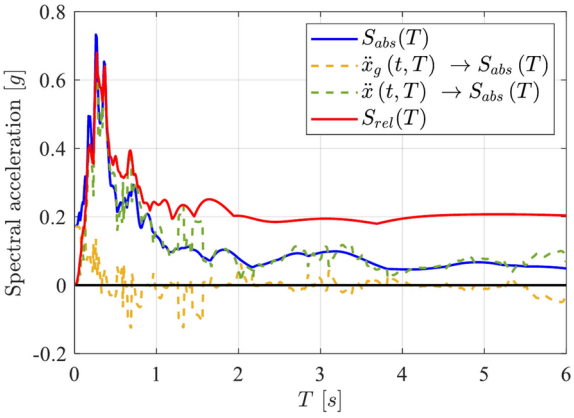

Fig. 10 Absolute and relative response acceleration with a PGA of 0.172 g for different time periods of SDOF system of the Loma Prieta Earthquake along with the components of the absolute response accelerations as $\ddot{x}_g(t,T)$ and $\ddot{x}(t,T)$

of $\ddot{x}(t)$ may not accurately represent its actual characteristics. This represents the challenge in employing the relative acceleration spectra. Furthermore, the legitimate reason that is getting carry forward on why the relative response spectrum for the flexible design of LST cannot be used is the superposition problem which is discussed in Sect. 4.5. Apart from superposition: the lack of consistency (due to site specific ground motion) and complexity of spectrum construction are further drawbacks.

4 Force-based approach

Chapter 4 addresses the basic criteria for the differentiation between rigid and flexible design of LST under seismic action. Subsequently, the existing simplified methodologies for estimating base shear and different superposition rules are compared. The comparison leads to introduction of a unified force-based approach by adeptly integrating coefficients across different superposition rules. A parametric study is then conducted to evaluate the

base shear outcomes derived from the unified force-based approach against conventional existing methodologies. Thereby, the combination rules for seismic actions and superposition schemes are presented. The chapter culminates by demonstrating the application of the unified force-based in terms of impulsive pressure components as an integral advantage in the LST seismic design approach.

4.1 Criteria for rigid and flexible tanks

In case of soil-structure interaction (SSI), the increase in the time period and the variation in structure to soil-stiffness ratio of a superstructure depends on many dimensionless variables. One such variable is H/V_sT where H represents the height of the structure, V_s is the shear wave velocity in soil and T is the fundamental natural time period of a superstructure (Bielak 1974; Veletsos and Nair 1975). Likewise, to quantify the stiffness of a tank system, the parameter H/T is used and has a unit of m/s (Stewart et al. 2012). By rearranging Eq. 10 in terms of H/T it can establish a measurable indicator of a tank's stiffness or rigidity based on Eq. 24. It is important to clarify that H/T itself does not constitute the actual stiffness or rigidity of the tank system, but rather serves as an index to quantify it. Consequently, a greater value of H/T denotes a more rigid tank, attributable to a greater wall thickness to radius ratio s_w/R, a lower γ, and a higher modulus of elasticity E for the material.

$$\left(\frac{H}{T}\right) = \frac{\sqrt{s_w/R}}{\frac{2\ F\ (\gamma)}{\sqrt{\gamma}}\sqrt{\rho_L/E}} \tag{24}$$

Figure 11 depicts the tank rigidity indicators and their contour mapping. It shows that a slender tank with γ greater than 1 compared to a squat one (less than 1) can have the same rigidity indicator depending on γ, radius to wall thickness ratio η and radius of tank R. Calvi and Nascimbene (2023) suggest a user-friendly table that provides discrete distinctions between rigid and flexible tank according to η and γ. However, the distinction along

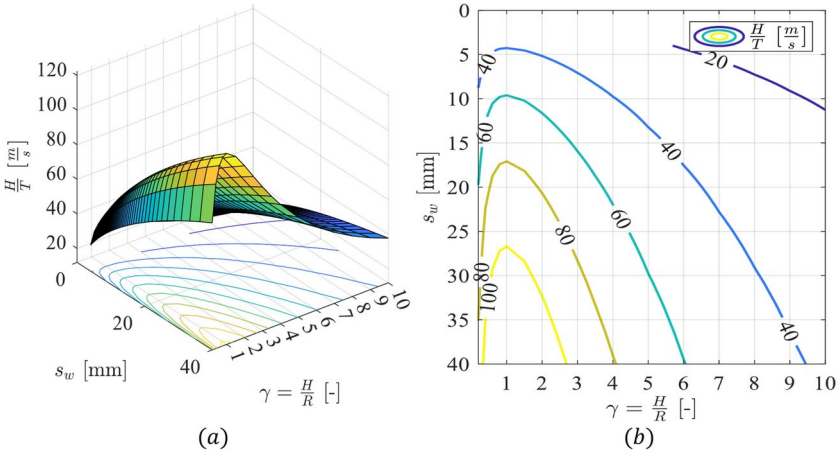

Fig. 11 **a** Tank rigidity indicators as inferred from Eq. 24 accompanied by their **b** corresponding contour maps for varying γ and s_w for a tank radius of 20 m

the diagonal of the table which is the dividing line between rigid and flexible design is indecisive. Despite the two variable distinction with η and γ, R of a tank also influences the fundamental time period and hence the response acceleration of the impulsive flexible component. This makes R as a third prominent variable in the flexible design. Furthermore, the impulsive masses depends on γ, η and unit weight of the contained liquid and container (Veletsos 1984). NZSEE (2009) neglects the later two parameters stating it as secondary importance for practical design purposes. This approach promotes a dichotomy in rigid and flexible design which ultimately manifests as a constraint. This is shown by the parametric study in Sect. 4.5 as a limitation of squat tank design.

4.2 Simplified calculation of base shear

This section explores detailed and simplified procedures for determining base shear and available superposition schemes to combine the components. Various approaches are available in EN 1998-4 (2006) to estimate base shear as shown in Table 1. The SRSS superimposed base shear expression in EN 1998-4 (2006) is given in Eq. 25.

$$F_{b,h}(t) = \sqrt{\left[\sum_{n=1}^{\infty} m_{cn}\ \ddot{x}_{cn}\,(t)\right]^2 + \left[m_{ir}\ \ddot{x}_g\,(t)\right]^2 + \left[m_{if}\ \ddot{x}_{abs}\,(t)\right]^2} \tag{25}$$

To begin with, for the relevant frequencies of the liquid storage tanks, the absolute and relative accelerations does not differ much. Based on this fact, Scharf (1990a) proposed the expression for base shear in the time-history domain shown in Eq. 26.

$$F_{b,h}(t) \ = \ \sum_{n=1}^{\infty} m_{cn}\ddot{x}_{cn}(t, T_{cn}) + m_{ir}\ddot{x}_g(t) + m_{if}\ \ddot{x}_{abs}(t, T_{if,h}) \tag{26}$$

Furthermore, Fischer et al. (1991) suggested 3 superposition schemes (A, B, and C) for calculating peak responses using spectral accelerations. The calculation of maximum base shear at $\cos\theta \ = \ 0°$ for different superposition schemes are given in Eqs. 27, 28 and 29 respectively.

Table 1 Expressions to calculate total base shear using flexible design approach

S. No.	Procedure based on	Base shear $F_{b,h}(t)$
1	Veletsos (1984) [a]	$\sum_{n=1}^{\infty} m_{cn}\ddot{x}_{cn}\,(t) + m_{imp}\ \ddot{x}_{abs}\,(t)$
2	Haroun and Housner (1981)	$\sum_{n=1}^{\infty} m_{cn}\ddot{x}_{cn}\,(t) + \left(m_{ir} - m_{if}\right)\ \ddot{x}_g\,(t) + m_{if}\ \ddot{x}_{abs}\,(t)$
3	Fischer et al. (1991) [b]	$\sum_{n=1}^{\infty} m_{cn}\ddot{x}_{cn}\,(t) + m_{ir}\ \ddot{x}_g\,(t) + m_{if}\ \ddot{x}_{abs}\,(t)$
4	Malhotra et al. (2000) [a]	$m_c\ S_{abs}\,(T_c) + m_{imp}\ S_{abs}\left(T_{if,h}\right)$

[a] $m_{imp} = m_{ir}$

[b] only at relavent typical frequency range of tank-fluid system

Superposition rule A: Fischer and Rammerstorfer (1982)

$$F_{b,h}|_A = \sqrt{\left[\sum_{n=1}^{\infty} m_{cn}\ S_{abs}\left(T_{cn}\right)\right]^2 + \left[m_{ir,h}\ S_{abs}\left(T_{ir,h}\right) + m_{if,h}\left(S_{abs}\left(T_{if,h}\right) - S_{abs}\left(T_{ir,h}\right)\right)\right]^2} \quad (27)$$

Superposition rule B: Rammerstorfer et al. (1988)

$$F_{b,h}|_B = \sqrt{\left[\sum_{n=1}^{\infty} m_{cn}\ S_{abs}\left(T_{cn}\right)\right]^2 + \left[m_{ir,h}\ S_{abs}\left(T_{ir,h}\right)\right]^2 + \left[m_{if,h}\ S_{abs}\left(T_{if,h}\right)\right]^2} \quad (28)$$

Superposition rule C:

$$F_{b,h}|_C = \sqrt{\left[\sum_{n=1}^{\infty} m_{cn}\ S_{abs}\left(T_{cn}\right)\right]^2 + \left[m_{ir,h}\ S_{abs}\left(T_{ir,h}\right)\right]^2 + \left[m_{if,h}\ S_{rel}\left(T_{if,h}\right)\right]^2} \quad (29)$$

Moreover, EN 1998-4 (2006) suggests an SRSS rule in a response spectral form for estimating total impulsive base shear (similar to superposition rule B) as given in Eq. 30:

$$F_{b,h,imp} = \sqrt{\left\{m_{ir} S_{abs}(T_{ir,h})\right\}^2 + \left\{m_{if}\ S_{abs}(T_{if,h})\right\}^2} \quad (30)$$

The key issue is whether Eqs. 26–30 accurately calculate base shears for both rigid and flexible design. In case of rigid design it works satisfactory, as m_{if} can be equated to zero leaving only the impulsive rigid term. However, in case of flexible design, the equations fail. For instance, if the rigidity is not known in advance, a high frequency tank ($T_{if,h} \approx 0$) using Eq. 30 will lead to approximately $\sqrt{2}$ times the impulsive rigid component (overestimated). Similarly, for a highly flexible tank, Eq. 30 does not have the elimination of the impulsive rigid term leading to inaccuracies. It is unseemly to use Eqs. 26–30 for relevant frequencies which not only depends on the tank characteristics but also soil conditions in case of SSI effects. For instance, $T_{ir,h}$ and $T_{if,h}$ are modified by the supporting soil stiffness. As a result $T_{ir,h}$ which would typically be assumed as zero for a rigid tank is no longer valid. In order to reformulate, instead of absolute response acceleration $S_{abs}(T_{if,h})$ for impulsive flexible term, relative response acceleration $S_{rel}(T_{if,h})$ can be used. But the use of relative response spectra is difficult as discussed in Chapter 3. Another way of estimating the impulsive base shear is given in Eq. 31 (Haroun and Housner 1981; NZSEE 2009). The major change here is the use of difference in impulsive rigid and flexible equivalent mass for the impulsive rigid component.

$$F_{b,h}(t) = \sum_{n=1}^{\infty} m_{cn}\ddot{x}_{abs}(t, T_{cn}) + (m_{ir} - m_{if})\ \ddot{x}_g(t) + m_{if}\ \ddot{x}_{abs}(t, T_{if,h}) \quad (31)$$

Despite the effectiveness of the formulation, the precise definition of the equivalent impulsive rigid mass is not consistently utilized. In case of rigid tank design it is defined as impulsive mass "m_{ir}" and in case of flexible tank design it is defined as rigid impulsive mass "$m_{ir} - m_{if}$". This characterization is also a skeptic means of describing the impulsive rigid hydrodynamic pressure distribution on the tank wall. Furthermore, the utilization of the relative acceleration for the impulsive flexible component is absent. Another simplified approach of estimating base shear is given in Eq. 32. While this approach provides convenient estimates of base shear (or overturning moments), it is inadequate for determining the corrected pressure distribution, particularly for flexible tanks.

$$F_{b,h}(t) \;=\; \sum_{n=1}^{\infty} m_{cn}\ddot{x}_{abs}(t, T_{cn}) + m_{ir}\;\ddot{x}_{abs}(t, T_{if,h}) \tag{32}$$

4.3 Unified force-based approach

A unified force-based approach is characterized by the integration of rigid and flexible design principles into a single approach using tabulated pressure and force coefficients which eliminates the distinction between these two design methodologies. When employing a unified force-based approach, the impulsive flexible component is consistently utilized without the necessity for checking the rigid or flexible design. If a tank is perfectly rigid, the flexible component becomes negligible, and conversely, if it is highly flexible, the total impulsive component vanishes. The consistent utilization of a well-defined methodology of liquid storage tank is a crucial aspect of the unified force-based approach. This also necessitates the use of relative acceleration in the impulsive flexible component particularly in response spectral format. This is described in the subsequent paragraphs.

In general, the symbol $\mathbb{R}$ is introduced to represent any peak structural response such as hydrodynamic pressure, base shear or overturning moment. The non-acceleration parameters associated with $\mathbb{R}$ are denoted by $\bar{\mathbb{R}}$. $\bar{\mathbb{R}}$ represents the convective, impulsive rigid, and impulsive flexible components of $\mathbb{R}$ without including the amplification effects caused by their respective response spectral accelerations. Therefore, $\mathbb{R}$ in a ABSSUM form can be written using Eq. 33:

$$\mathbb{R} = \sum_{n=1}^{\infty} \bar{\mathbb{R}}_{cn}\,|\ddot{x}_{cn}\,(t)|_{max} + \bar{\mathbb{R}}_{ir,h}\;\;|\ddot{x}_{g}\,(t)|_{max} + \;\bar{\mathbb{R}}_{if,h}\;\;|\ddot{x}\,(t)|_{max} \tag{33}$$

In order to use the relative response acceleration $|\ddot{x}\,(t)|_{max}$ in its spectral format, there are two possibilities. The first possibility is shown in Eq. 34 that defines the absolute maxima of the relative acceleration time history.

$$|\ddot{x}\,(t)|_{max} = \;\;|\ddot{x}_{abs}\,(t) - \ddot{x}_{g}\,(t)|_{max} \;\;\rightarrow S_{rel}\,(T_{if,h}) \tag{34}$$

However, the direct application of the relative response spectrum is challenging as explained in Chapter 3. The second possibility is given in Eq. 35 that defines the relative acceleration

as a difference of the individual absolute maxima of absolute and ground acceleration time history. This also forms the foundation of the unified force-based approach.

$$|\ddot{x}(t)|_{max} = \ |\ddot{x}_{abs}(t)|_{max} - \ |\ddot{x}_{g}(t)|_{max} \ \rightarrow S_{abs}(T_{if,h}) - S_{abs}(T_{ir,h}) \tag{35}$$

Eq. 35 becomes more intuitive and logical when directly combined with the impulsive rigid terms using the ABSSUM approach as shown in Eq. 36.

$$\mathbb{R} = \sqrt{\left[\sum_{n=1}^{\infty} \bar{\mathbb{R}}_{cn} \ S_{abs}(T_{cn})\right]^2 + \ \left[\bar{\mathbb{R}}_{ir,h} \ S_{abs}(T_{ir,h}) + \ \bar{\mathbb{R}}_{if,h}\{S_{abs}(T_{if,h}) - S_{abs}(T_{ir,h})\}\right]^2} \tag{36}$$

By using the difference in the absolute spectral acceleration and PGA for the impulsive flexible component (Eq. 35) and directly adding the impulsive flexible components with impulsive rigid components (Eq. 36) along with the superposition principle forms the core formulation of the unified force-based approach. For instance, in case of rigid tank, the impulsive flexible period $T_{if,h}$ closely approximates the impulsive rigid period $T_{ir,h}$, effectively reducing the contribution of the flexible component to zero. Conversely, in the case of a flexible tank, the relative acceleration is exclusively considered for the flexible component. When combined with the rigid component, ensures the overall impulsive response. This also aligns with the consistent definition of simplified impulsive equivalent masses with their corresponding response accelerations. For instance, the base shear using the force coefficients can be written as given in 37.

$$F_{b,h} \ = \sqrt{[F_{b,c}]^2 + \ [F_{b,ir,h} + \ F_{b,if,h}]^2} = \ \sqrt{[F_{b,c}]^2 + \ [F_{b,h,imp}]^2} \tag{37}$$

with:

$F_{b,c} \quad = C_{F,c} \ \Gamma_c \ m_L \ S_{abs}(T_c)$

$F_{b,ir,h} \quad = C_{F,ir,h} \ \Gamma_{ir,h} \ m_L \ S_{abs}(T_{ir,h})$

$F_{b,if,h} \quad = C_{F,if,h} \ \Gamma_{if,h} \ m_L \ \{S_{abs}(T_{if,h}) - S_{abs}(T_{ir,h})\}$

$F_{b,h,imp} \quad = F_{b,ir,h} + F_{b,if,h}$

4.4 Combination rules and superposition schemes

According to Karaferis and Vamvatsikos (2021) the amplification factor of the seismic action effect due to 2^{nd} horizontal component of the earthquake can be reduced from 30% to 12% into a unidirectional since the tanks are the axisymmetric structures. Therefore, the combination of the action effects due to horizontal earthquake E_{Edx} and the action effects due to vertical earthquake E_{Edz} in the SRSS (Square Root of the Sum of Squares) format for an on-ground vertical cylindrical tank is given in Eq. 38. The maximum of the two possible actions is taken. The factor 0.34 is the result of 0.30 x 1.12.

$$\begin{cases} \sqrt{\{1.12 \ E_{Edx}\}^2 + \{0.30 \ E_{Edz}\}^2} \\ \sqrt{\{0.34 \ E_{Edx}\}^2 + \{1.00 \ E_{Edz}\}^2} \end{cases} \tag{38}$$

Therefore, total hydrodynamic pressure $p_{hyd,w}$ acting on the wall due to combined horizontal and vertical seismic action is given as in Eq. 39.

$$p_{hyd,w} = max\left(\sqrt{\{1.12\ p_h\}^2 + \{0.30\ p_v\}^2}, \sqrt{\{0.34\ p_h\}^2 + \{1.00\ p_v\}^2}\right) \tag{39}$$

with:

$$p_h = \sqrt{{p_c}^2 + \{p_{ir,h} + p_{if,h}\}^2}$$

$$p_v = p_{ir,v} + p_{if,v}$$

Furthermore, the superposition schemes of the reactions i.e. base shear $F_{b,h}$, overturning moment (M_w and M_g) and vertical support reaction F_v of the unified force-base design approach is succinctly given in Eq. 40.

$$\begin{cases} F_{b,h} = \sqrt{\{F_{b,c}\}^2 + \{F_{b,ir,h} + F_{b,if,h}\}^2} \\ M_w = \sqrt{\{M_{w,c}\}^2 + \{M_{w,ir,h} + M_{w,if,h}\}^2} \\ M_g = \sqrt{\{M_{g,c}\}^2 + \{M_{g,ir,h} + M_{g,if,h}\}^2} \\ F_v = F_{ir,v} + F_{if,v} \end{cases} \tag{40}$$

4.5 Parametric study

To verify the consistency of the unified force-based approach, a parametric study is carried out. The peak structural response is selected as impulsive base shear. The focus remains only on the impulsive part as the convective component combinations remains same as other approaches. Tank geometries according to Table 2 are assumed. The height H and wall thickness s_w of the tank is adjusted to have corresponding aspect ratio γ and time period $T_{if,h}$ of the liquid tank.

The impulsive base shear according to the unified force-based approach is given in Eq. 41. It is imperative to add the two impulsive components in an ABSSUM format, as applying the SRSS method for the two components is not permissible. The notation used is "U" for unified design.

$$F_{b,h,imp}|_U = C_{F,ir,h}\ \Gamma_{ir,h}\ m_L\ S_{abs}(T_{ir,h}) + C_{F,if,h}\ \Gamma_{if,h}\ m_L\ \{S_{abs}(T_{if,h}) - S_{abs}(T_{ir,h})\} \tag{41}$$

The simplified equation for estimating impulsive base shear is given in Eq. 42 according to Malhotra et al. (2000). The notation used is "M".

$$F_{b,h,imp}|_M = m_{ir} S_{abs}(T_{if,h}) \tag{42}$$

Table 2 The liquid density and geometrical properties of the tank in parametric study

Radius	R	$[m]$	5
Density of liquid	ρ_L	$[\frac{t}{m^3}]$	1
Aspect ratio	$\gamma = \frac{H}{R}$	[-]	[0.2 0.6 1 2]
Time periods	$T_{if,h}$	$[s]$	[0.01 0.02 0.03.... 4]

All base shear estimation formulae offered in EN 1998-4 (2006) are presented in a time-history format, except for the incorporated superposition rule B. Although, the superposition rules described in Fischer et al. (1991) are for hydrodynamic pressure, the same rules are compared again with unified force-based approach for impulsive base shear and are shown in Eqs. 43–45. The notation used is "A", "B" and "C" respectively.

$$F_{b,h,imp}|_A = m_{ir} S_{abs}(T_{ir,h}) + m_{if} \{S_{abs}(T_{if,h}) - S_{abs}(T_{ir,h})\} \tag{43}$$

$$F_{b,h,imp}|_B = m_{ir} S_{abs}(T_{ir,h}) + m_{if}\ S_{abs}(T_{if,h}) \tag{44}$$

$$F_{b,h,imp}|_C = m_{ir} S_{abs}(T_{ir,h}) + m_{if}\ S_{rel}(T_{if,h}) \tag{45}$$

To ensure consistency in comparison, the superposition rules B and C are evaluated in ABSSUM format. The primary distinction between the superposition rule A and superposition scheme from unified force-based approach is the estimation of the impulsive equivalent masses using force coefficients instead of iteration of Bessel functions which has not been carried forward to any design codes till present.

The expression of impulsive base shear presented in NZSEE (2009) is given in Eq. 46. In essence, Eq. 46 demonstrates the differentiation between the rigid and flexible design of tanks solely in terms of γ. The notation used is "N".

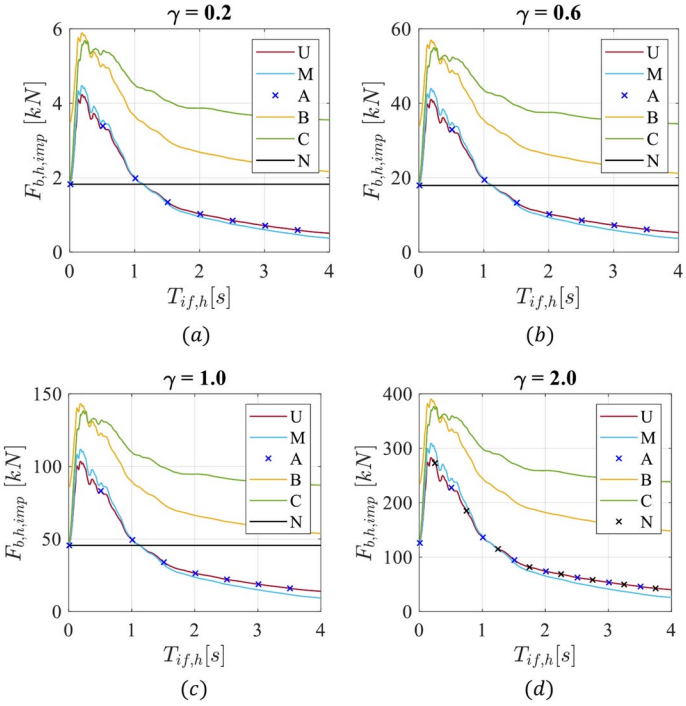

Fig. 12 Impulsive base shear $F_{b,h,imp}$ for different γ for a tank radius $R = 5\ m$. comparing approaches

$$\begin{cases} F_{b,h,imp}|_N &= m_{ir} S_{abs}(T_{ir,h}) \; \forall \; \gamma \; \leq \; 1 \\ F_{b,h,imp}|_N &= \{m_{ir} - m_{if}\} \; S_{abs}(T_{ir,h}) + \; m_{if} S_{abs}(T_{if,h}) \; \forall \; \gamma \; > \; 1 \end{cases} \tag{46}$$

The mean absolute acceleration spectra shown in Fig. 9 is used for the study. The PGA is taken as $0.21g$.

Figure 12 plots the impulsive base shear $F_{b,h,imp}$ for different $T_{if,h}$ and γ of a tank. Initially, Fischer et al. (1991) demonstrated that the superposition rule B or C can be applied for liquid storage tanks across a broad frequency range. This is accomplished by utilizing the absolute and relative response spectra respectively. Nevertheless, a universal trend exists in the response spectra, wherein the velocity sensitive range demonstrates a convergence of the maxima of both the absolute and relative spectra as illustrated in Fig. 12 a to d. However, this seems overestimated when compared to the base shear values from Malhotra et al. (2000). The utilization of superposition rule in EN 1998-4 (2006) often overlooks the significance of superposition rule A. As shown in Fig. 12a, it aligns with the simplified methodology proposed by Malhotra et al. (2000) for wide range of different γ and impulsive flexible time period of tanks.

Figure 12 a to d demonstrates that the base shears resulting from the application of superposition rule B (Eq. 44) are overestimated for rigid tanks exactly by $\sqrt{2}$ times. Furthermore, even for highly flexible tanks, the impulsive component does not diminish since superposition rule B does not eliminate the impulsive rigid component. As a result, base shear estimates naturally approaches the value of $T_{if,h} = 0$ again, which does not make physically sense for flexible tanks. It is impossible to eliminate the impulsive rigid and flexible components through superposition using the SRSS rule, as they must be counterbalanced in opposite phase at higher time periods.

The base shear estimates from superposition rule C (Eq. 45) are valid only in the acceleration sensitive regions of the spectra. Although as discussed in Chapter 3, it is recommended to avoid the use of relative spectra. The condition $S_{rel}\,(T_{if,h}) \approx S_{abs}\,(T_{if,h})$ is also0 satisfied in the velocity sensitive region of the spectra, as depicted in Fig. 12 which results in the $F_{b,h,imp}$ values aligning with superposition rule B but does not matches again with the approach by Malhotra et al. (2000). In the displacement sensitive region of the response spectra for higher time periods, the impulsive component does not disappear and is substantially overestimated. This is due to the fact that maxima of relative spectral acceleration $S_{rel}\,(T_{if,h})$ for impulsive flexible component starts approaching the $S_{abs}\,(T_{ir,h})$.

Equation 46 makes a distinction between rigid and flexible design approach in terms of γ. As shown in Fig. 12 a to c, due to rigid design the base shear is constant for $\gamma \leq 1$. The consideration of wall thickness flexibility is an important aspect to be included in the seismic design of squat tanks as suggested by Calvi and Nascimbene (2023). This limitation in the existing guidelines indicates a need for further research and development in order to ensure the safe and efficient seismic design of squat tanks. In spite of the limitation for squat tanks, Eq. 46 starts following the same trend as with the unified force-based approach for $\gamma > 1$ as shown in Fig. 12d.

The base shear estimates from Eq. 42 matches well with the unified force-based approach as shown in Fig. 12. The difference in the approach is the use of single (impulsive rigid mass) and double (impulsive rigid and flexible masses) - SDOF oscillator for simplified and unified force-based approach respectively. The base shear estimates from unified force-based approach are a marginally lower for lower time periods in comparison to Eq. 42 because of

the consideration of impulsive flexible masses, which are observed to be consistently lower than impulsive rigid masses. The effect is vice-versa for higher time periods.

To summarize, the base shear from the unified force-based approach keeping the consistent definition intact to each impulsive component works well and are in line with Malhotra et al. (2000), superposition rule A from Fischer et al. (1991) and NZSEE (2009) for $\gamma > 1$. However, when applying the superposition rule B and C, it has been observed that inconsistent results may occur for a wide range of time periods. The similar trend can be observed for overturning moments.

4.6 Inherence nature of unified force-based approach

The subsequent study is conducted with a view to verify the procedure of unified force-based approach for the simplified hydrodynamic pressure distribution in particular to impulsive flexible component. In order to see the effects of tank rigidity for squat tanks ($\gamma < 1$) another parametric study is performed. The main aim is to check the contribution of hydrodynamic impulsive rigid and flexible pressure distribution for different γ and s_w of the tank shell. The geometric and material properties remain unchanged from those detailed in Table 2, and the loading conditions are in accordance with the mean absolute acceleration spectra presented in Fig. 9 with a PGA of $0.21g$. For the analysis of pressure function, the time period given in Eq. 10 is used. The impulsive rigid and impulsive flexible pressure is calculated using Eqs. 47 and 48 in their response spectral acceleration format as per the unified force-based method.

$$p_{ir,h}(\xi = 1, \theta = 0^\circ, \zeta) \;=\; R\;\rho_L\;C_{ir,h}(\gamma,\zeta)\;S_{abs}(T_{ir,h})\;\Gamma_{\mathrm{ir,h}} \tag{47}$$

$$p_{if,h}(\xi = 1, \theta = 0^\circ, \zeta) \;=\; R\;\rho_L\;C_{if,h}\,(\gamma,\zeta)\;\{S_{abs}\,(T_{if,h}) - S_{abs}\,(T_{ir,h})\}\;\Gamma_{\mathrm{if,h}} \tag{48}$$

The time period $T_{if,h}$ contour obtained for different γ and s_w shown in Fig. 13a clearly shows for higher wall thickness and lower aspect ratios of tank the time period are small and vice-versa. It also shows the indication of the rigidness of two tanks can remain the same (shown as contour) depending on γ and s_w. The respective position of absolute acceleration with respect to PGA i.e. acceleration amplification factor is also shown in Fig. 13b. Clearly,

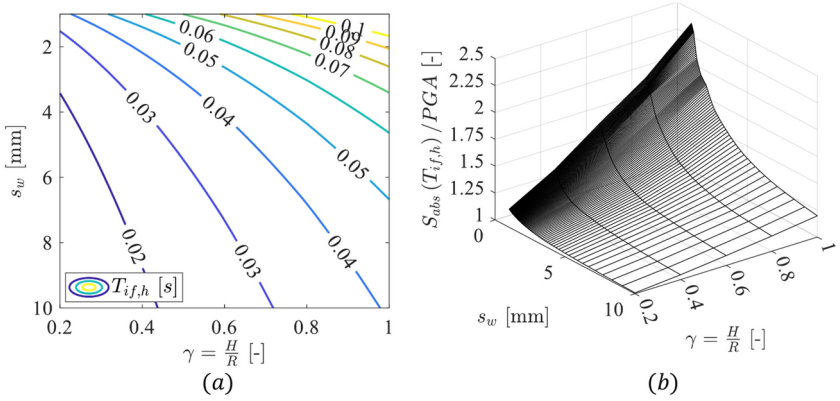

Fig. 13 **a** Tank period contour for squat tanks and **b** respective response acceleration with respect to PGA

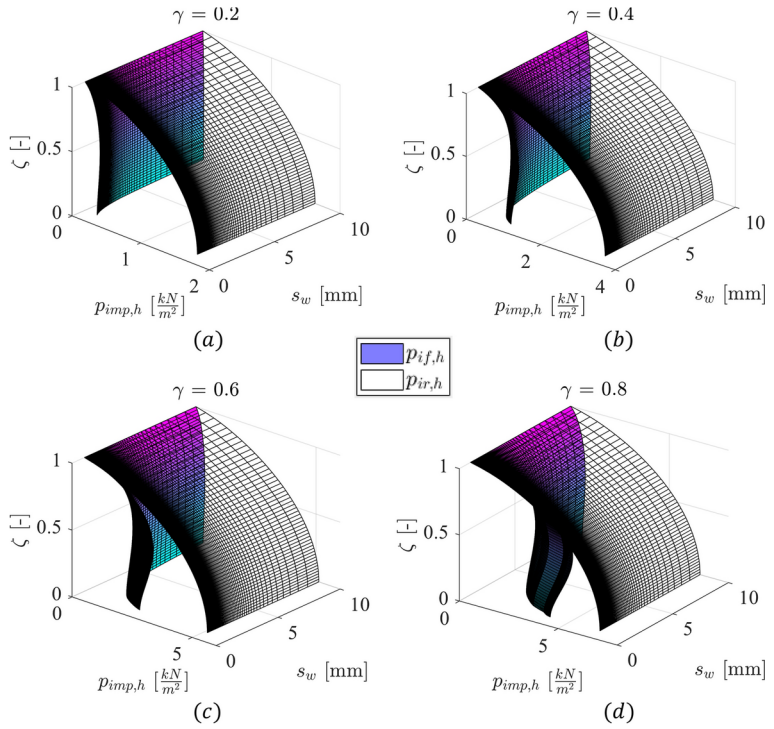

Fig. 14 Impulsive pressure distribution (rigid and flexible component) for different γ and s_w

the tanks with lower time periods $T_{if,h}$ (rigid tanks) will lie closer to the initial phase of response spectrum i.e. PGA. Here, $T_{if,h} = 0$ corresponds to value 1.0. As the time period of the tank increases, corresponding response acceleration starts following the normalized response spectrum surface shown in Fig. 13b in 3D for different γ and s_w of the tank.

The plots of resulting impulsive rigid and impulsive flexible hydrodynamic pressure for ($\gamma \leq 1$) are shown in Fig. 14a to d. Figure 14a clearly shows steel tank with thicker wall thickness, the impulsive flexible pressures function are low and even close to zero for squat tanks. As the γ of the tank increases, impulsive flexible pressure starts dominating for thinner wall sections (Fig. 14 b to c). For thicker wall sections, an appreciable amount of flexible component still exist for higher γ. Although, it is important to note that in case of slender tanks, higher modes becomes decisive and the unified force-base approach is limited to only one eigen mode only. With further increase in γ, the impulsive flexible pressure increases as seen in Fig. 14d. The plots for squat tanks clearly identifies the impulsive flexible component that increase with γ and decrease with s_w. The study shows that the differentiation of rigid and flexible tank design mere on the basis of γ is clearly controversial.

With the use of unified force-based approach, the flexibility of liquid storage tank in terms of its γ, s_w and a corrected hydrodynamic impulsive pressure distribution is implemented. The differentiation between the tanks with respect to γ is no longer required as it can represent all the tank configuration inherently. The dominating impulsive flexible pressures in squat tanks gets unified to the impulsive pressure and hence rigid design is eliminated.

Table 3 Parameter of the fluid-tank system according to Manos and Clough (1982)

Nomenclature	Symbol	Unit	Squat tank
Geometrical properties			
Inner radius	R	$[m]$	1.83
Total height	L	$[m]$	1.83
Fluid height	H	$[m]$	1.53
Aspect ratio	γ	[-]	0.84
Wall thickness shell course 1	s_{w1}	$[mm]$	2.0
Wall thickness shell course 2	s_{w2}	$[mm]$	1.3
Fluid properties (Water)			
Fluid density	ρ_L	$[\frac{t}{m^3}]$	1.0
Fluid mass	m_L	$[t]$	16.1
Tank properties (Aluminium)			
Material density	ρ_T	$[\frac{t}{m^3}]$	2.7
Young's modulus of elasticity	E	$[GPa]$	71
Yield strength	f_y	$[MPa]$	100

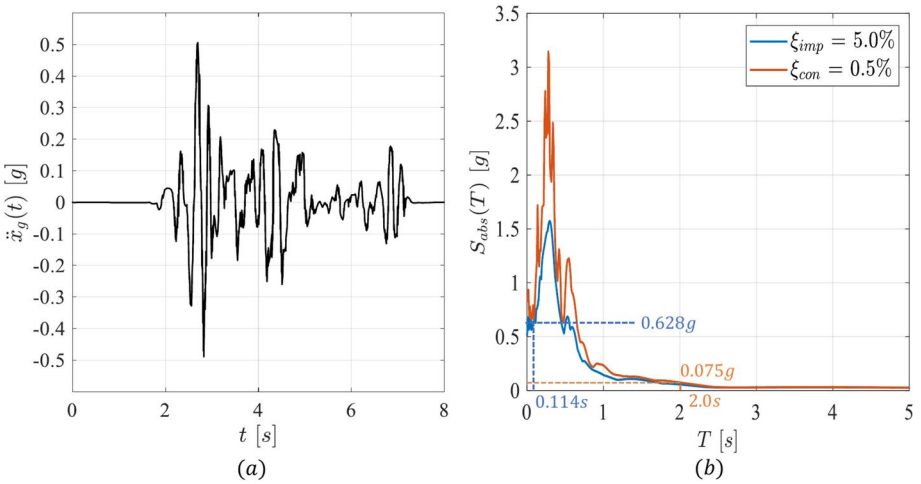

Fig. 15 Horizontal table acceleration and its acceleration response spectra for 0.5% and 5% as sloshing and impulsive damping

5 Validation

In order to validate the unified force-based approach formulation, the experimental results from Manos and Clough (1982) and the same tank extended with FEM results from Ozdemir et al. (2010) are utilized as a benchmark. Table 3 shows the material and geometrical properties of the tank model used in the experiment. The open-top, broad tank was a 1/3 scale model of a steel prototype, made up of aluminum with an L-shaped girder placed on the second shell course. The horizontal shaking motion with a peak table acceleration of $0.5g$ of the El Centro 1940 earthquake was applied which was also scaled with regard to time by $1/\sqrt{3}$ because of similitude requirements.

Figure 15a shows the horizontal table acceleration and Fig. 15b shows acceleration response spectra for 0.5% and 5% as sloshing and impulsive damping respectively. The acceleration response spectra were created using the average acceleration method using the Newmark approach from Vamvatsikos (2011) that matched the spectra according to Ozdemir et al. (2010). Also, the fundamental time period obtained from the experiment and corresponding response acceleration to impulsive and convective motions are shown in Fig. 15b. The response acceleration is later used to validate the unified force-based approach formulation.

The two-step validation is carried forward. In the first step, the coefficients in Chapter 2 for (hydrodynamics pressure, base shear, and overturning moment) are applied to the experimental tank for validating the coefficients in the time series domain. In the second step, the validated coefficients with the unified force-based approach formulation are compared with the experimental maximum values.

5.1 First stage validation of coefficients in time domain

The time history of hydrodynamic pressure observed in the experiment at $0.05\ m\,(\zeta = 0.033$) height above the tank base is used for validation. The effect of the convective pressure component near the base of the tank is negligible and hence neglected. Equations 49–51 show the impulsive rigid, impulsive flexible, and combined hydrodynamic pressure equation with coefficients for the selected experimental tank respectively.

$$p_{ir,h}(\xi = 1, \zeta = 0.033, \theta = 0^{\circ}, t) = R\ \rho_L\ C_{ir,h}\,(\gamma, \zeta)\ \ cos\theta\ \ddot{x}_g\,(t) \tag{49}$$

$$p_{if,h}(\xi = 1, \zeta = 0.033, \theta = 0^{\circ}, t) = R\ \rho_L\ C_{if,h}\,(\gamma, \zeta)\ \ cos\theta\ \ddot{x}\,(t, T_{if,h},\ \xi_{imp}) \tag{50}$$

$$p_{imp,h}(t) = p_{ir,h}(t) + p_{if,h}(t) \tag{51}$$

The aspect ratio γ of the broad tank is calculated as 0.84. The interpolated impulsive rigid $C_{ir,h}$ and impulsive flexible $C_{if,h}$ hydrodynamic pressure coefficients for $\zeta = 0.033$ are calculated as listed in Table 4. Likewise, the interpolated impulsive rigid $\Gamma_{ir,h}$ and impulsive flexible $\Gamma_{if,h}$ participation factors are given in Table 4. The ground acceleration $\ddot{x}_g\,(t)$ is used for the impulsive rigid component whereas the relative acceleration $\ddot{x}\,(t)$ for the experimentally obtained impulsive mode period $T_{if,h} = 0.114\ s$ and impulsive damping $\xi_{imp} = 5\%$ is calculated using the approach shown in Chapter 3.

Table 4 The interpolated tabular coefficients for $\gamma = 0.84$

Coefficients	Symbol	Mode		
		Convective $(j = c)$	Impulsive rigid $(j = ir, h)$	Impulsive flexible $(j = if, h)$
Hydrodynamic pressure at $(\zeta = 0.033)$	C_j	0.346	0.652	0.247
Base shear	$C_{F,j}$	0.518	0.479	0.26
Overturning moment (wall)	$C_{MW,j}$	0.304	0.192	0.12
Participation factor	Γ_j	1	1	1.638

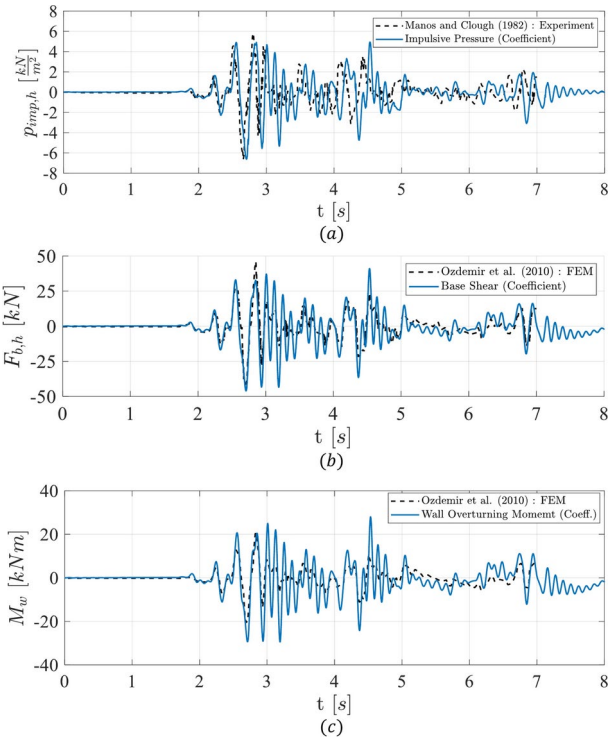

Fig. 16 Comparision of **a** impulsive pressure, **b** base shear, and **c** overturning moment time histories of the experimental tank

Figure 16a compares the experimentally obtained pressure close to the base of the tank and the hydrodynamic impulsive pressure calculated using the pressure coefficients. The pressure magnitudes are in close correlation and are consistently predicted. The maximum pressure magnitude also matches. Likewise, the coefficient-derived base shear and the overturning moment are compared with the numerical FEM analysis performed by Ozdemir et al. (2010). In this comparison, the base shear and overturning moment due to the sloshing are now considered.

The expressions given in Eq. 40 were used for the calculation of base shear and wall overturning moment using the unified force-based approach. Figure 16 b and c shows the corresponding time series plot of base shear and overturning moment respectively.

5.2 Second stage validation of unified force-based approach with response spectrum

The second stage of validation concentrates on implementing the unified force-based approach in response spectrum format by incorporating the previously validated tabular coefficients. As stated earlier, the approach offers a simplified formulation for computing hydrodynamic pressure components and stress resultants by utilizing acceleration response spectra. The acceleration component in the time history is replaced with the spectral response acceleration corresponding to the respective fundamental mode. In this case, the response spectra presented in Fig. 15b is applied to calculate the spectral accelerations and further absolute maximum values of the hydrodynamic pressure, base shear, and overturn-

Table 5 Response parameters of the experimental tank

Parameter	Units	Experiment	FEM	Coefficient Tables	Unified force-based approach	API 650 (2013)	EN 1998-4 (2006)		NZSEE (2009)
		Manos and Clough (1982)	Ozdemir et al. (2010)			Housner (1963)	Veletsos and Yang (1977)	Malhotra et al. (2000)	Veletsos (1984)
$p_{h,max}$	kN/m^2	6.665	5.912	6.620	6.808	-	-	-	-
$F_{b,h,max}$	*kN*	-	46.08	46.04	46.84	38.7	50.1	53.1	40.8
$M_{w,max}$	*kNm*	27.50	20.64	29.43	29.32	23.8	34.1	37.2	26.7

ing moment. For the convective and impulsive rigid component, the respective spectral response accelerations, namely $S_{abs}(T_c) = 0.075g$ and $S_{abs}(T_{ir,h}) = 0.506g$, are applied. Furthermore, as explained in Chapter 4, for the impulsive flexible component, the difference between absolute spectral response acceleration, i.e., $S_{abs}(T_{if,h}) = 0.628g$, and rigid spectral response acceleration $S_{abs}(T_{ir,h})$ is used which turns out to be 0.122 *g* (Table 5).

The comparison of the results commences with an examination of the hydrodynamics pressure function. Notably, the absolute maxima of the experimental hydrodynamic pressure function at the base of the tank match with the result obtained using the unified force-based approach with a little conservative error of 2%. Moreover, the numerically derived base shear obtained by Ozdemir et al. (2010), approximately 46 kN, correlates precisely with the tabulated coefficients as well as the unified force-based approach. It becomes evident that the base shear values derived from API 650 (2013) and NZSEE (2009) are notably underestimated due to the rigid design approach. Conversely, the approach presented by Malhotra et al. (2000), despite adopting a flexible design, slightly overestimates the base shear value due to the consideration of only impulsive rigid mass. Furthermore, a similar observation can be made regarding the overturning moment. The unified formulation utilizing the response spectrum yields considerably fair results aligning well with the experimental values.

6 Application

The unified force-based design approach allows for straightforward calculation of seismic demands as demonstrated in Chapter 4. Furthermore, a significant benefit lies in the ability to utilize the unified hydrodynamic pressure distribution as a quasi-static equivalent loadm enabling the estimation of meridian and circumferential stresses for the tank geometry. This approach proves highly advantageous, leading to substantial time savings by avoiding exhaustive fluid–structure interaction simulations. In this chapter, two examples are shown using the FEM software InfoCAD (2024) to showcase an application wherein the hydrodynamic pressure, calculated through a unified force-based approach is applied as a quasi-static equivalent load to evaluate the increase in stresses and base shear as shown in Fig. 17.

The tank base and wall are modeled using shell elements (SH46). The application of the total hydrodynamic pressure p_h involves imposing area element loads as quasi static loads on each shell element as shown in Fig. 17. The magnitude of the area load varies along the depth of the liquid height as well as the in the circumferential direction with a cosine function. The initial example utilizes the identical experimental tank (squat tank with $\gamma \leq 1$) from the previous chapter (Chapter 5). In contrast, the subsequent example demonstrates the systematic application of the unified force-based approach for a considerably slender tank ($\gamma > 1$).

6.1 Example 1

The numerical model employs the same tank (open-top, fixed support condition) dimensions and material properties as those used in the experimental study as shown in Table 3. In the tank model, the wall thickness is maintained uniformly at 2 *mm*. It is important to note that this tank model represents a scaled-down experimental version, as a thickness of 2 *mm*

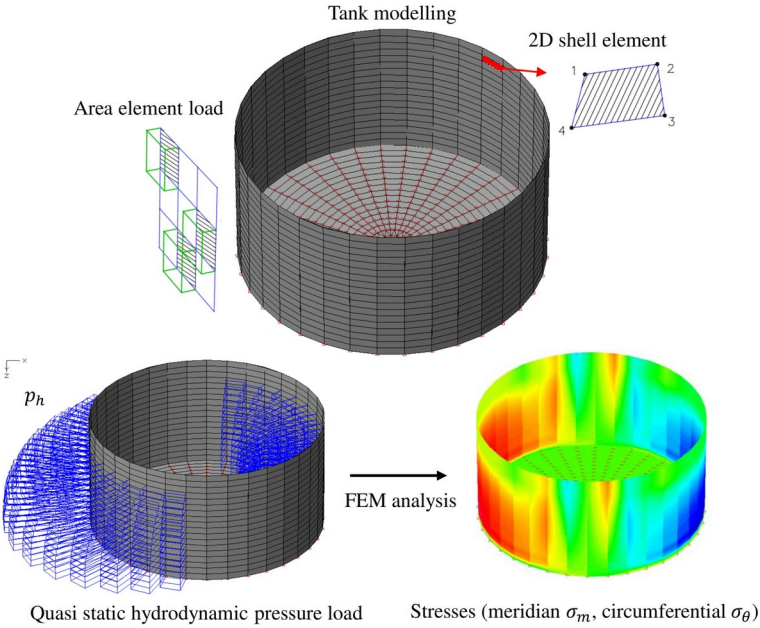

Fig. 17 Quasi-static application of the hydrodynamic pressure on the FEM tank model using InfoCAD (2024)

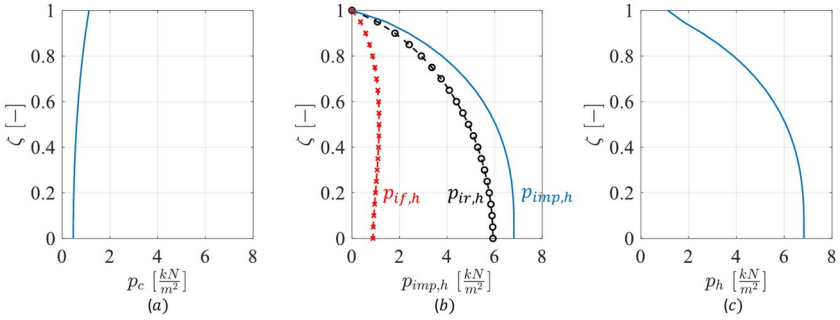

Fig. 18 Hydrodynamic pressure distribution of each component and combined pressure p_h at $\theta = 0°$ due to horizontal seismic excitation

is significantly less than what is found in realistic applications. To ensure brevity, geometric and material linearity is applied, considering that the observed meridian stresses in the experimental study remained well within the elastic limit. The pressure coefficients convective C_c, impulsive rigid $C_{ir,h}$ and impulsive flexible $C_{if,h}$ are interpolated for $\gamma = 0.84$. Thereby, the distribution of the calculated hydrodynamic pressure components along the height of the tank for $\theta = 0°$ is shown in Fig. 18. The time periods and response spectral accelerations for each component, as detailed in Sect. 5.2, remain unchanged.

The example combines the impulsive flexible $p_{if,h}$ and impulsive rigid $p_{ir,h}$ components using the unified force-based formulation (see Eq. 36). Figure 18b shows that the impulsive

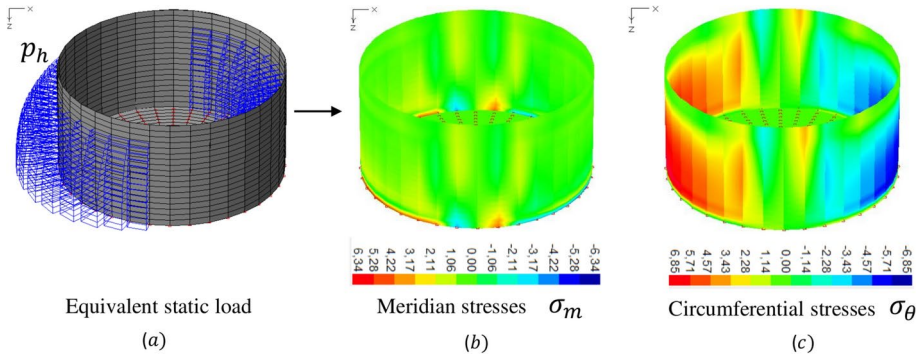

Equivalent static load (*a*) Meridian stresses σ_m (*b*) Circumferential stresses σ_θ (*c*)

Fig. 19 Application of equivalent static load to the squat tank wall and corresponding distribution of meridian stresses and circumferential stresses at the tank

Table 6 Comparison of base shear and maximum axial membrane stress due to hydrodynamic pressure for different approaches

Approach/Literature	Base shear (kN)	Shell axial membrane stress (MPa)
FEM/(Unified force-based approach)	47.6	6.34
Formulation/(Unified force-based approach)	46.8	–
Experiment/Manos and Clough (1982)	–	4.90
FEM/Ozdemir et al. (2010)	46.1	3.30
API 650 (2013)/Housner (1954)	38.7	1.25
EN 1998-4 (2006)/Veletsos and Yang (1977)	50.1	1.77
EN 1998-4 (2006)/Malhotra et al. (2000)	53.1	1.93
NZSEE (2009)/Veletsos (1984)	40.8	1.40

flexible pressure component is smaller compared to the impulsive rigid pressure component but exhibits a non-zero distribution attributable to the squat tank. The SRSS is employed to combine the convective p_c and impulsive hydrodynamic pressure components $p_{imp,h}$ to get total hydrodynamic pressure p_h as shown in Fig. 18c. This resulting pressure p_h is then applied as an area element load to the tank wall as shown in Fig. 19 to calculate meridian and circumferential stresses.

As presented in Table 6, the numerically calculated base shear $47.6\ kN$ approximately matches with the analytically derived base shear $46.8\ kN$, confirming the accurate application of the total hydrodynamic pressure load. The quasi-static analysis indicates that compressive meridional stresses are concentrated at the bottom of the tank wall, reaching a value of 6.34 MPa. This value is slightly higher than the experimentally derived compressive meridional stress of 4.9 MPa. Conversely, equal and opposite tensile meridional stress is observed at the opposite end of the tank. In Table 6, the compressive meridional stresses obtained from alternative approaches, sourced from Ozdemir et al. (2010) are also presented. It has been observed that the compressive meridional stress values derived from these other approaches were found to be underestimated. The potential cause for this discrepancy could be attributed to the variation in the calculation of the impulsive flexible time period, resulting in lower spectral acceleration values and consequently reduced compressive meridional stresses. Furthermore, stresses from Housner (1963) approach are under-

estimated due to neglecting of the impulsive flexible pressure. However, by employing the hydrodynamic loads as a static load through FEM and adopting a unified rigid and flexible design approach an adequate estimation of the stresses within the tank system is achieved, thereby circumventing time-consuming calculations.

6.2 Example 2

In this example, the systematic implementation of the unified force-based approach is applied to a slender steel tank from Meskouris et al. (2019). DIN 4149 (2005) response spectrums are applied for the consistent comparison between the literatures. The base shear, overturning moment (wall), overturning moment (wall and base) for each hydrodynamic pressure components are calculated. Subsequently, after deriving pressure components, the hydrodynamic pressure functions are applied as an equivalent static load to the numerical tank model (Table 7). Finally, the response parameters are evaluated and compared.

The vibration periods are calculated using the expressions provided in Chapter 2 and hence the convective T_c, impulsive rigid period $T_{ir,h}$, and impulsive flexible eigenperiod $T_{if,h}$ were 2.26 s, 0 s and 0.34 s respectively. FprEN 1998-4 (2025) suggests the use of the elastic spectrum for the convective component, whereas the design (or reduced) spectrum $(q = 1, 2)$ for the impulsive component. Therefore, the corresponding elastic spectral acceleration $S_{abs}\,(T_c)$ for the convective component is 0.354 $\frac{m}{s^2}$. Since the impulsive rigid period is 0s, the design (or reduced) response spectral acceleration $S_{abs}\,(T_{ir,h})$ is equal to 0.54 $\frac{m}{s^2}$. In the case of an impulsive flexible component, the absolute reduced response spectral acceleration $S_{abs}\,(T_{if,h})$ turns out to be 1.125 $\frac{m}{s^2}$ (Fig. 20).

The difference between the spectral accelerations $S_{abs}\,(T_{if,h}) - S_{abs}\,(T_{ir,h})$ which equals 0.585 $\frac{m}{s^2}$ is used in order to calculate the impulsive flexible pressure components as per unified force-based approach. The tabulated pressure coefficient C_j, along with the force and moment coefficients ($C_{F,j}$, $C_{MW,j}$, $C_{M,j}$) and the participation factor Γ_j, where $(j = \{c; ir, h; if, h\})$ were extracted for $\gamma = 6$. These coefficients were utilized to compute

Table 7 Parameters of the fluid-tank system (Meskouris et al. 2019)

Nomenclature	Symbol	Unit	Slender tank
Tank properties			
Inner radius	R	[m]	2.35
Tank length	L	[m]	15.75
Liquid height	H	[m]	14.1
Aspect ratio	$\gamma = \frac{H}{R}$	[–]	6
Wall thickness	s_w	[mm]	3.7
Young's modulus of elasticity	E	[GPa]	170
Fluid properties			
Fluid density	ρ_L	$[\frac{t}{m^3}]$	1.35
Liquid mass	m_L	[t]	330.25
Seismic loading			
Importance factor	γ_i	[–]	1.2
Spectrum class			C-S
PGA	a_g	$[\frac{m}{s^2}]$	0.6
Convective damping	ξ_c	[%]	0.5
Behavior Factor	q	[–]	1.2

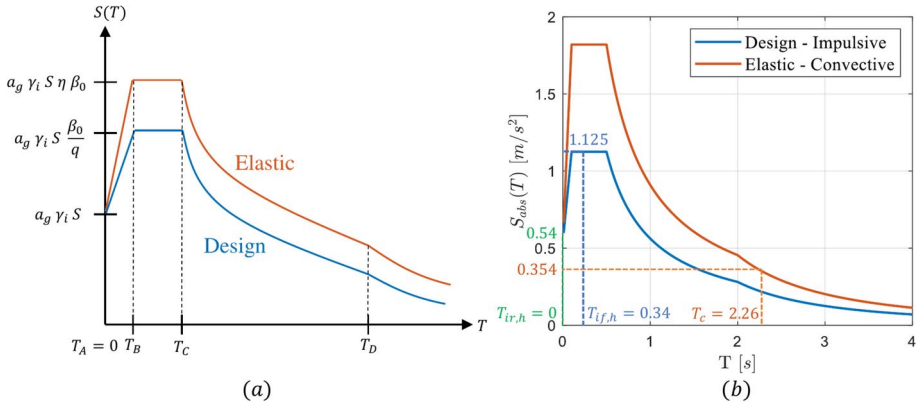

Fig. 20 **a** Design (reduced) and elastic response spectra according to DIN4149 (2005), **b** Design and elastic response spectra for impulsive and convective component respectively with eigen periods and spectral accelerations for each pressure component

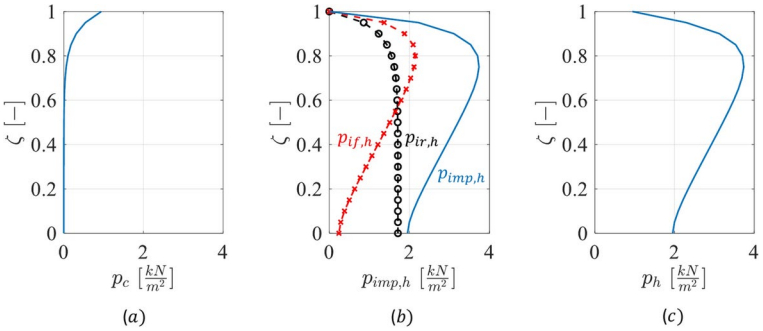

Fig. 21 Hydrodynamic pressure distribution of each component and combined pressure p_h at $\theta = 0°$ due to horizontal seismic excitation

the hydrodynamic pressure components and were superimposed using unified approach to have total hydrodynamic pressure p_h, as illustrated in Fig. 21.

The upper half of the tank shell experiences a greater concentration of total hydrodynamic pressure p_h due to a significant impulsive flexible response acceleration. The base shear and overturning moments from the unified force-based approach are compared with the other literature's as shown in Table 8. It is to be noted that the impulsive components are typically summed before applying the SRSS rule to integrate the convective and impulsive components. However, in Meskouris et al. (2019), Malhotra et al. (2000), and Housner (1963), each component are combined using the SRSS rule individually. Due to the minimal impact of the convective pressure, the following paragraph centers on comparing the impulsive components. The impulsive flexible base shear and moments outcomes from Meskouris et al. (2019) as (228.7 *kN*, 2056.9 *kNm*, 2060.1 *kNm*) are higher relative to the unified force-based approach (135.1 *kN*, 1165.0 *kNm*, 1167.7 *kNm*), primarily because they employ superposition rule B which leads to overestimation (see Sect. 4.5). Interestingly, the combined superposition results closely align with those from the unified force-based

Table 8 Comparison of the total base shear and overturning moments

	Parameter	Unit	Unified force-based approach	Iterative added mass FEM	Simplified procedure	Rigid design
			FprEN 1998-4 (2025)	Meskouris et al. (2019)	Malhotra et al. (2000)	Housner (1963)
	Notation:		(j = c | ir,h | if,h)	(j = c | ir,h | if,h)	(j = c | imp,h)	(j = c | ir,h)
Hydro-dynamic Component	Acceleration	$[\frac{m}{s^2}]$	0.354 | 0.540 | 0.585	0.354 | 0.540 | 1.125	0.354 | 1.125	0.354 | 0.54
	Γ_j	[−]	1.0 | 1.0 | 1.63	2.0 | 1.0 | 1.67	-	-
	$F_{b,j}$	[*kN*]	9.2 | 164.2 | 135.1	17.9 | 160.9 | 228.7	8.9 | 342.1	6.4 | 172.9
	$M_{w,j}$	[*kNm*]	118.3 | 1075.7 | 1165.0	118.3 | 1049.6 | 2056.9	113.7 | 2241.4	81.9 | 1137.8
	$M_{g,j}$	[*kNm*]	118.3 | 1093.2 | 1167.7	118.3 | 1066.5 | 2060.1	113.7 | 2277.7	81.9 | -
Superposition (SRSS)	F_b	[*kN*]	299.4	280.2	342.3	172.9
	M_w	[*kNm*]	2243.8	2312.2	2244.2	1140.8
	M_g	[*kNm*]	2264.0	2322.8	2280.6	-

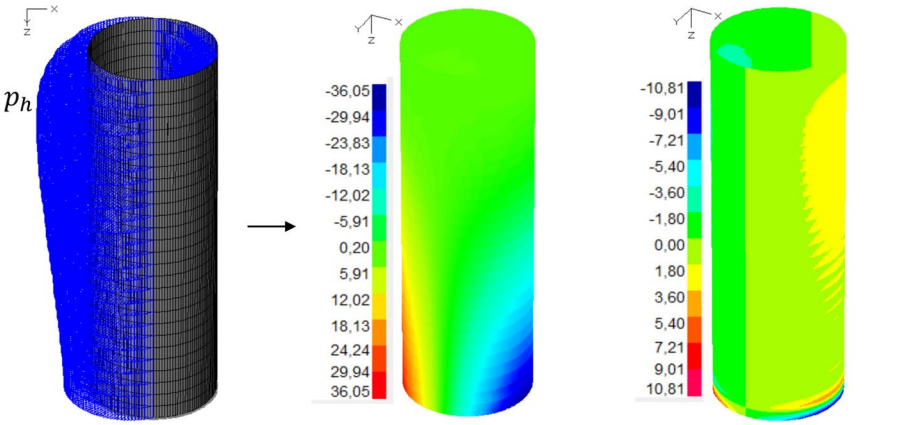

Fig. 22 Application of equivalent static load to the slender tank wall and corresponding distribution of meridian stresses and circumferential stresses at the tank

approach. This similarity arises because the unified force-based approach involves summing the impulsive components directly, while in Meskouris et al. (2019), the individual components are combined using the SRSS method resulting in comparable outcomes. In comparison with Malhotra et al. (2000), the combined base shear of 342.3 *kN* is overestimated compared to the unified force-based approach 299.4 *kN* because of the exclusive use of the impulsive rigid mass m_{ir} in the simplified procedure. Regarding overturning moments, there is a good match between the approaches. This matching in moments can be attributed to the fact that in the unified force-based approach, the equivalent height of the impulsive flexible component is higher, while in the simplified procedure the impulsive rigid height is

lower, resulting in a balanced outcome for the overturning moments. Since $m_{if} < m_{ir} \; \forall \; \gamma$, the estimated forces and moments are more effectively calculated in FprEN 1998-4 (2025).

In the FEM model, the wall thickness is maintained uniformly at 3.7 *mm*. To ensure brevity, geometric and material linearity is applied. The total hydrodynamic pressure function p_h was applied as an equivalent static load to the slender tank FEM model as shown in Fig. 22. The maximum meridian stress obtain was 36.05 *MPa* that concentrated at the bottom of the tank. Unlike the previous example, the stress distribution extended more towards the upper part of the shell, attributing to the tank's higher γ and reduced s_w. Similarly, the maximum circumferential stress recorded was 10.81 *MPa*. Both stress values fall well within the elastic limit.

In conclusion, this chapter effectively demonstrates the application of the unified force-based approach through two distinct examples, highlighting the use of total hydrodynamic pressure as an equivalent static load. This method ensures an easy path and comprehensive understanding of stress distributions within the tank walls. Such quasi static load application, particularly in the context of redesigning tank geometries and conditions, underscores the versatility of the unified formulation. It offers significant time savings to designers, streamlining the process of adapting designs to meet specific structural requirements while ensuring accuracy and reliability in stress analysis.

7 Conclusion

The paper critically examined classification of the above ground LST into rigid and flexible tanks present in the existing codes and proposed a unified force-based design approach for seismic analysis of such tanks. Different methodologies proposed in the codes and literature demonstrated limitations in practicality and accuracy with issues in employing complex iterative procedures, simplified relative accelerations for impulsive flexible component, evaluating impulsive flexible pressures, and defining equivalent impulsive masses for rigid and flexible tanks. The analysis of response spectral components for flexible design of LST revealed that the simultaneous application of spectral ground and relative acceleration without altering impulsive component definitions is a significant challenge and leads to under or overestimates of seismic demands. By scrutinizing the definitions of hydrodynamic impulsive components, the parametric study revealed inconsistencies in estimating total base shear and overturning moments for different tank geometries when applying various superposition rules across different time periods.

The unified force-based approach introduced a formulation for applying simplified relative accelerations to impulsive flexible components by utilizing existing pressure coefficients and spectral acceleration with correct superposition scheme intending to provide a streamlined alternative to distinct definitions to rigid and flexible design. It standardizes the treatment of LST by combining aspect ratio γ, wall thickness, and hydrodynamic impulsive pressure thereby eliminating the need for rigid design distinctions across different aspect ratio and wall thickness ratio. The two stage validation of the unified force-based approach through the results of a previously conducted research showed that the estimation of maximum pressure, stress resultants, and meridian stresses were in close proximity. The application of this formulation has been demonstrated through a quasi-static finite element numerical study on squat and slender tanks. The use of quasi-static load application by

applying total hydrodynamic pressure as an equivalent static load, especially for tank redesigns, underscores the quick estimation of seismic stresses. The study also forms the basis for the new generation of Eurocode EN 1998-4 which is demonstrated for different tank geometries. In future research endeavors, it is essential to extend the scope of investigation to encompass unanchored tanks, as their behavior remains a critical area of interest. Additionally, exploring various superposition principles for both rigid and flexible tanks with soil-structure interaction can enhance the applicability of the formulation across different scenarios.

Acknowledgements The authors wish to express their gratitude to their colleagues, the reviewers, and Professor Dimitrios Vamvatsikos for their valuable comments and suggestions, which significantly contributed to the improvement of this manuscript.

Funding Open Access funding enabled and organized by Projekt DEAL.
This research did not receive any specific grant from funding agencies in the public, commercial, or not-for-profit sectors.

Data availability The generated data during the current study are available from the corresponding author on reasonable request.

Declarations

Conflict of interest The authors declare that there are no Conflict of interest regarding the publication of this paper.

References

Ancheta TD, Darragh RB, Stewart JP, et al (2013) PEER NGA-West2 Database. Technical Report PEER 2013/03, Pacific Earthquake Engineering Research Center, Berkeley, California, https://apps.peer.berkeley.edu/publications/peer_reports/reports_2013/webPEER-2013-03-Ancheta.pdf

API 650 (2013) Welded Tanks for Oil Storage. Tech. rep., American Petroleum Institute, Washington, D.C., https://archive.org/details/API65012th2013

Aziz M (2021) Liquid hydrogen: a review on liquefaction, storage, transportation, and safety. Energies 14(18):5917. https://doi.org/10.3390/en14185917

Bielak J (1974) Dynamic behaviour of structures with embedded foundations. Earthq Eng Struct Dyn 3(3):259–274. https://doi.org/10.1002/eqe.4290030305

Brunesi E, Nascimbene R, Pagani M et al (2015) Seismic performance of storage steel tanks during the May 2012 Emilia, Italy, earthquakes. J Perform Constr Facil 29(5):04014137. https://doi.org/10.1061/(ASCE)CF.1943-5509.0000628

Calvi GM, Nascimbene R (2023) Seismic design and analysis of tanks, 1st edn. Wiley, New York

Caprinozzi S, Paolacci F, Bursi OS et al (2021) Seismic performance of a floating roof in an unanchored broad storage tank: experimental tests and numerical simulations. J Fluids Struct 105:103341. https://doi.org/10.1016/j.jfluidstructs.2021.103341

Chang JI, Lin CC (2006) A study of storage tank accidents. J Loss Prev Process Ind 19(1):51–59. https://doi.org/10.1016/j.jlp.2005.05.015
Clough DP (1977) Experimental evaluation of seismic design methods for broad cylindrical tanks. Dissertation (Ph.D.), University of California, Berkeley, California, https://api.semanticscholar.org/CorpusID:109036221
Clough RW, Niwa A, Clough DP (1979) Experimental seismic study of cylindrical tanks. J Struct Div 105(12):2565–2590. https://doi.org/10.1061/JSDEAG.000531
Cornelissen P (2010) Erarbeitung eines vereinfachten impulsiv-flexiblen Lastansatzes für die Berechnung von Tankbauwerken unter Erdbebenlast. Dissertation (Ph.D.), RWTH Aachen University, Aachen, Germany
Danciu L, Nandan S, Reyes C, et al (2021) The 2020 update of the European seismic hazard model: model overview. Tech. Rep. 001, EFEHR, Zurich, Switzerland, https://doi.org/10.12686/a15
DIN 4149 (2005) Buildings in German Earthquake Areas - Design Loads, Analysis and Structural Design of Buildings. Deutsches Institut für Normung, Berlin, Germany, https://www.dinmedia.de/de/norm/din-4149/78232028
EN 1998–4 (2006) Eurocode 8 - Design of Structures for Earthquake Resistance - Part 4: Silos. Tanks and Pipelines, European Committee for Standardization (CEN), Brussels, Belgium
Epstein HI (1976) Seismic design of liquid-storage tanks. J Struct Div 102(9):1659–1673. https://doi.org/10.1061/JSDEAG.0004421
Erdik M (2001) Report on 1999 Kocaeli and Düzce (Turkey) Earthquakes. Structural Control for Civil and Infrastructure Engineering pp 149–186. https://doi.org/10.1142/9789812811707_0018
Erkmen B (2024) Seismic performance assessment of an existing anchored and a self-anchored liquid storage tank in high seismic regions. Bull Earthq Eng 22:4197–4217. https://doi.org/10.1007/s10518-024-01932-x
Fischer F (1979) Dynamic fluid effects in liquid-filled flexible cylindrical tanks. Earthq Eng Struct Dyn 7(6):587–601. https://doi.org/10.1002/eqe.4290070608
Fischer F (1981) Ein Vorschlag zur erdbebensicheren Bemessung von flüssigkeitsgefüllten zylindrischen Tankbauwerken. Der Stahlbau 50:13–20
Fischer FD, Rammerstorfer FG (1999) A refined analysis of sloshing effects in seismically excited tanks. Int J Press Vessels Pip 76(10):693–709. https://doi.org/10.1016/S0308-0161(99)00047-2
Fischer F, Seeber R (1988) Dynamic response of vertically excited liquid storage tanks considering liquid–soil interaction. Earthq Eng Struct Dyn 16(3):329–342. https://doi.org/10.1002/eqe.4290160304
Fischer FD, Rammerstorferf F, Scharf K (1991) Earthquake resistant design of anchored and unanchored liquid storage tanks under three-dimensional earthquake excitation. Springer, Berlin
Fischer F, Rammerstorfer FG (1982) The stability of liquid-filled cylindrical shells under dynamic loading. Buckling of shells: proceedings of a state-of-the-art colloquium. Springer, Stuttgart, pp 569–597
Girgin S, Necci A, Krausmann E (2019) Dealing with cascading multi-hazard risks in national risk assessment: the case of Natech accidents. Int J Disast Risk Reduct 35:101072. https://doi.org/10.1016/j.ijdrr.2019.101072
González E, Almazán J, Beltrán J et al (2013) Performance of stainless steel winery tanks during the 02/27/2010 Maule Earthquake. Eng Struct 56:1402–1418. https://doi.org/10.1016/j.engstruct.2013.07.017
Habenberger J (2001) Beitrag zur Berechnung von nachgiebig gelagerten Behältertragwerken unter seismischen Einwirkungen. Dissertation (Ph.D.), Bauhaus-Universität Weimar, https://doi.org/10.25643/bauhaus-universitaet.44, https://www.db-thueringen.de/servlets/MCRFileNodeServlet/dbt_derivate_00041692/Habenberger_pdfa.pdf
Hackbusch W, Schwarz HR, Zeidler E (2003) Teubner-taschenbuch der mathematik, 2nd edn. Springer, Berlin
Haroun MA (1980) Dynamic Analyses of Liquid Storage Tanks. Dissertation (Ph.D.), California Institute of Technology, Pasadena, California, https://doi.org/10.7907/1J74-RH65, https://resolver.caltech.edu/CaltechTHESIS:08292019-100431566
Haroun M, Housner G (1981) Earthquake response of deformable liquid storage tanks. J Appl Mech 48(2):411–418. https://doi.org/10.1115/1.3157631
Holl HJ (1987) Parameteruntersuchung zur Abgrenzung der Anwendbarkeit eines Berechnungskonzeptes für Erdbebenbeanspruchte Tankbauwerke. Dissertation (Ph.D.), TU Wien, Wien, Austria
Holtschoppen B, Knoedel P (2024) Seismic response of slender storage tanks on tube feet or skirt support. Bull Earthq Eng 22(1):55–73. https://doi.org/10.1007/s10518-023-01704-z
Housner GW (1954) Earthquake pressures on fluid containers. California Institute of Technology, Pasadena
Housner GW (1963) The dynamic behavior of water tanks. Bull Seismol Soc Am 53(2):381–387. https://doi.org/10.1785/BSSA0530020381
InfoCAD (2024) InfoCAD version: 21.0(b). https://www.infograph.eu/

Jacobsen LS (1949) Impulsive hydrodynamics of fluid inside a cylindrical tank and of fluid surrounding a cylindrical pier. Bull Seismol Soc Am 39(3):189–204. https://doi.org/10.1785/BSSA0390030189
Jacobsen LS, Ayre RS (1951) Hydrodynamic experiments with rigid cylindrical tanks subjected to transient motions. Bull Seismol Soc Am 41(4):313–346. https://doi.org/10.1785/BSSA0410040313
Karaferis N, Vamvatsikos D (2021) Seismic action combination rules for the design of azimuth-independent structures. In: Proceedings of the 8th international conference on computational methods in structural dynamics and earthquake engineering, pp 5134–5141, https://doi.org/10.7712/120121.8854.18598
Kettler M (2004) Earthquake Design of Large Liquid-Filled Steel Storage Tanks. Dissertation (Ph.D.), TU Graz, https://graz.elsevierpure.com/de/publications/earthquake-design-of-large-liquid-filled-steel-storage-tanks
Krausmann E, Cruz AM (2013) Impact of the 11 March 2011, great East Japan earthquake and tsunami on the chemical industry. Nat Hazards 67:811–828. https://doi.org/10.1007/s11069-013-0607-0
Lau D, Clough R (1989) Static Tilt Behavior of Unanchored Cylindrical Tanks, Report, vol 89. Earthquake Engineering Research Center, University of California, https://books.google.de/books?id=1d9HAQAAIAAJ
Luft RW (1984) Vertical accelerations in prestressed concrete tanks. J Struct Eng 110(4):706–714. https://doi.org/10.1061/(ASCE)0733-9445(1984)110:4(706)
Malhotra PK (2021) Seismic response of liquid-storage tanks. Springer, Cham
Malhotra PK, Wenk T, Wieland M (2000) Simple procedure for seismic analysis of liquid-storage tanks. Struct Eng Int 10(3):197–201. https://doi.org/10.2749/101686600780481509
Manos GC, Clough RW (1982) Further study of the earthquake response of a broad cylindrical liquid-storage tank model. UCB/EERC 82/07, University of California, Earthquake Engineering Research Center
Manos GC (1991) Evaluation of the earthquake performance of anchored wine tanks during the San Juan, Argentina, 1977 earthquakes. Earthq Eng Struct Dyn 20(12):1099–1114. https://doi.org/10.1002/eqe.4290201202
MATLAB (2023) MATLAB version: 23.2.0.2365128 (R2023b). https://www.mathworks.com
Meskouris K, Butenweg C, Hinzen KG et al (2019) Structural dynamics with applications in earthquake and wind engineering, 2nd edn. Springer, Aachen
Meskouris K, Hinzen KG, Butenweg C et al (2011) Bauwerke und erdbeben: grundlagen - anwendung - beispiele, 3rd edn. Springer, Aachen
Natsiavas S (1987) Response and Failure of Fluid-Filled Tanks under Base Excitation. Dissertation (Ph.D.), California Institute of Technology, Pasadena, California, https://doi.org/10.7907/CNWT-V417, https://resolver.caltech.edu/CaltechETD:etd-11062007-092509
Niwa A (1978) Seismic behavior of tall liquid storage tanks. Dissertation (Ph.D.), University of California, Berkeley, California
NZSEE (2009) Seismic Design of Storage Tanks: 2009. New Zealand Society for Earthquake Engineering, Recommendations of a NZSEE Study Group on Seismic Design of Storage Tanks
Ozdemir Z, Souli M, Fahjan Y (2010) Application of nonlinear fluid-structure interaction methods to seismic analysis of anchored and unanchored tanks. Eng Struct 32(2):409–423. https://doi.org/10.1016/j.engstruct.2009.10.004
Paolacci F, Butenweg C, Vamvatsikos D (2024) SI: Natech risk assessment of hazardous facilities. Bull Earthq Eng 22(1):1–4. https://doi.org/10.1007/s10518-023-01799-4
Park JH, Bae D, Oh CK (2016) Experimental study on the dynamic behavior of a cylindrical liquid storage tank subjected to seismic excitation. Int J Steel Struct 16:935–945. https://doi.org/10.1007/s13296-016-0172-y
Phan HN, Paolacci F, Filippo RD et al (2020) Seismic vulnerability of above-ground storage tanks with unanchored support conditions for Na-Tech risks based on Gaussian process regression. Bull Earthq Eng 18:6883–6906. https://doi.org/10.1007/s10518-020-00960-7
prEN 1998–4 (2025) Eurocode 8 - Design of Structures for Earthquake Resistance - Part 4: Silos, Tanks and Pipelines, Towers. Masts and Chimneys, European Committee for Standardization (CEN), Brussels, Belgium
Priestley M, Wood J, Davidson B (1986) Seismic design of storage tanks. Bull N Z Soc Earthq Eng 19(4):272–284. https://doi.org/10.5459/bnzsee.19.4.272-284
Rammerstorfer FG, Scharf K, Fischer F et al (1988) Collapse of earthquake excited tanks. Res Mech 25(2):129–143
Rammerstorfer FG, Scharf K, Fischer FD (1990) Storage tanks under earthquake loading. Appl Mech Rev 43(11):261–282. https://doi.org/10.1115/1.3119154
Rammerstorfer F, Fischer F (2004) Ein Vorschlag zur Ermittlung von Belastungen und Beanspruchungen von zylindrischen, flüssigkeitsgefüllten Tankbauwerken bei Erdbebeneinwirkung. In: Neuauflage des Institutsberichtes ILFB-2/90. Report, TU Wien, Wien, Austria

Scharf K (1990a) Beiträge zur Erfassung des Verhaltens von erdbebenerregten, oberirdischen Tankbauwerken. Fortschritt-Berichte VDI. Reihe 4, Bauingenieurwesen, VDI-Verlag, Wien, Austria, https://katalog.slub-dresden.de/id/0-017248329

Scharf K (1990b) Contributions to response monitoring of surface tank structures under seismic stress. Beitraege zur Erfassung des Verhaltens von erdbebenerregten, oberirdischen Tankbauwerken. Dissertation (Ph.D.), TU Wien, Wien, Austria

Schiff AJ (1991) Guide to post-earthquake investigation of lifelines. U.S. Department of Energy Office of Scientific and Technical Information, https://www.osti.gov/biblio/6993643

Shih CF (1981) Failure of Liquid Storage Tanks due to Earthquake Excitation. Dissertation (Ph.D.), California Institute of Technology, Pasadena, California, https://doi.org/10.7907/m0v8-hs31, https://resolver.caltech.edu/CaltechTHESIS:04132018-090928397

Shih CF, Babcock CD (1987) Buckling of oil storage tanks in SPPL tank farm during the 1979 imperial valley earthquake. J Press Vessel Technol 109(2):249–255. https://doi.org/10.1115/1.3264904

Sigloch H (2012) Fluid-dynamik, grundlagen, 8th edn. Springer, Berlin, pp 63–130

Stempniewski L (1990) Flüssigkeitsgefüllte Stahlbetonbehälter unter Erdbebeneinwirkung. Dissertation (Ph.D.), Karlsruhe Institute of Technology, Karlsruhe, Germany

Stewart J, Crouse C, Hutchinson T, et al (2012) Soil-structure interaction for building structures. Grant/Contract Reports (NISTGCR), National Institute of Standards and Technology, Gaithersburg, MD, https://tsapps.nist.gov/publication/get_pdf.cfm?pub_id=915495

Swan SW, Miller DD, Yanev PI (1985) The Morgan Hill earthquake of April 24, 1984-effects on industrial facilities, buildings, and other facilities. Earthq Spectra 1(3):457–568. https://doi.org/10.1193/1.1585276

Tang Y (1986) Studies of Dynamic Response of Liquid Storage Tanks (Foundations, Rings, Vibration, Discs). Dissertation (Ph.D.), Rice University, Houston, Texas

Vamvatsikos D (2011) IDA Matlab running routines for OpenSEES. GNU General Public License, http://users.ntua.gr/divamva/software.html, Accessed: 2021-07-15

Vamvatsikos D, Cornell CA (2004) Applied incremental dynamic analysis. Earthq Spectra 20(2):523–553. https://doi.org/10.1193/1.1737737

Veletsos A (1974) Seismic effects in flexible liquid storage tanks. In: Proceedings of the 5th world conference on earthquake engineering, bulletin of the seismological society of America McLean, Rome, Italy, pp 630–639, https://www.iitk.ac.in/nicee/wcee/article/5_vol1_630.pdf

Veletsos A (1984) Seismic response and design of liquid storage tanks. Guidelines for the seismic design of oil and gas pipeline systems. American Society of Civil Engineers, New York, pp 255–370

Veletsos AS, Yang J (1976) Dynamics of fixed base liquid storage tanks. In: Proceedings of US-Japan seminar on earthquake engineering research with emphasis on lifeline systems, Japan Society for Promotion of Earthquake Engineering, Tokyo, pp 317–341

Veletsos AS, Yang J (1977) Earthquake response of liquid storage tanks. In: Proceedings of the second engineering mechanics specialty conference. ASCE, Raleigh, NC, pp 1–24

Veletsos AS, Nair VD (1975) Seismic interaction of structures on hysteretic foundations. J Struct Div 101(1):109–129. https://doi.org/10.1061/JSDEAG.0003962

Veletsos A, Tang Y (1986) Dynamics of vertically excited liquid storage tanks. J Struct Eng 112(6):1228–1246. https://doi.org/10.1061/(ASCE)0733-9445(1986)112:6(1228)

Wozniak RS, Mitchell WW (1978) Basis of seismic design provisions for welded steel oil storage tanks. In: Session on advances in storage tank design. American Petroleum Institute

Yanagisawa E, Yasuda S, Mori S et al (1990) Loma Prieta earthquake damage investigation reconnaissance report on the Loma Prieta earthquake of October 17, 1989. J Jpn Soc Civil Eng 424:19–68. https://doi.org/10.2208/jscej.1990.424_19

Yoshida S (2018) Earthquake damages and disaster prevention of aboveground storage tanks. EPI Int J Eng 1(2):87–93. https://doi.org/10.25042/epi-ije.082018.14

Yu CC, Whittaker AS (2020) Analytical solutions for seismic fluid-structure interaction of head-supported cylindrical tanks. J Eng Mech 146(10):04020112. https://doi.org/10.1061/(ASCE)EM.1943-7889.0001831

Authors and Affiliations

Soumitra Chatterji[1] · Christoph Butenweg[2] · Sven Klinkel[1]

✉ Soumitra Chatterji
chatterji@lbb.rwth-aachen.de

Christoph Butenweg
butenweg@cwe.rwth-aachen.de

Sven Klinkel
klinkel@lbb.rwth-aachen.de

[1] Chair of Structural Analysis and Dynamics, RWTH Aachen University, Mies-van-der-Rohe-Straße 1, 52074 Aachen, North Rhine-Westphalia, Germany

[2] Center for Wind and Earthquake Engineering, RWTH Aachen University, Mies-van-der-Rohe-Straße 1, 52074 Aachen, North Rhine-Westphalia, Germany